Contrib Mineral Petrol (2014) 168:1069
DOI 10.1007/s00410-014-1069-4

ORIGINAL PAPER

Boron isotopes in tourmaline as a tracer of metasomatic processes in the Bamble sector of Southern Norway

R. Bast · E. E. Scherer · K. Mezger · H. Austrheim · T. Ludwig · H. R. Marschall · A. Putnis · K. Löwen

Received: 23 December 2013 / Accepted: 18 September 2014 / Published online: 10 October 2014

Abstract The Bamble sector of southern Norway comprises metagabbros and metasediments that were metasomatically altered to various extents during a late stage of the Sveconorwegian orogeny (~1.06 Ga). The infiltration of highly saline brines along veins led to penetrative scapolitization and albitization on a regional scale and the local deposition of Fe–Ti oxides. Typical secondary mineral assemblages include either scapolite + apatite + amphibole + phlogopite + tourmaline, or albite + epidote + calcite + chlorite + white mica, indicating that the fluids introduced large amounts of Na, Cl, Mg, Ca, K, P, and B to the system. Metasomatic tourmalines associated with different alteration stages as identified by variations in major-element composition and initial $^{87}Sr/^{86}Sr$ were analyzed for B isotopic compositions to constrain possible sources and the evolution of the hydrothermal fluid(s). Measured $\delta^{11}B$ values range from −5 to +27 ‰ relative to SRM-951, suggesting marine evaporites interlayered with various amounts of continental detritus and pelagic clay as a possible B source reservoir. The influence of a seawater-derived component is clearly indicated by the heavy B isotope signature of tourmaline related to Al–Mg-rich metapelites. In contrast, negative $\delta^{11}B$ values can be explained by the influence of pneumatolytic fluids associated with granitic pegmatites. On a regional scale (i.e., several km), $\delta^{11}B$ values in tourmaline vary widely, whereas variations within a single outcrop (tens of m) are typically small and can be ascribed to different generations of tourmaline related to several fluid pulses.

Keywords Boron isotopes · Tourmaline · Bamble sector · Metasomatism · Fluid source · Strontium isotopes

Communicated by T. L. Grove.

Electronic supplementary material The online version of this article (doi:10.1007/s00410-014-1069-4) contains supplementary material, which is available to authorized users.

R. Bast (✉) · E. E. Scherer · K. Mezger · A. Putnis · K. Löwen
Institut für Mineralogie, Westfälische Wilhelms-Universität Münster, Corrensstraße 24, 48149 Münster, Germany
e-mail: Rebecca.Bast@uni-muenster.de

K. Mezger
Institut für Geologie, Universität Bern, Baltzerstraße 1+3, 3012 Bern, Switzerland

H. Austrheim
Physics of Geological Processes, University of Oslo, Sem Sælands vei 24, 0316 Oslo, Norway

T. Ludwig
Institut für Geowissenschaften, Universität Heidelberg, Im Neuenheimer Feld 234-236, 69120 Heidelberg, Germany

H. R. Marschall
Department of Geology and Geophysics, Woods Hole Oceanographic Institution, MS #8, Woods Hole, MA 02543, USA

Introduction

Hydrous fluids play a key role during metamorphic processes. They promote mineral reactions, aid in the achievement of thermodynamic equilibrium among minerals, and may result in complete recrystallization under ambient P–T conditions during prograde metamorphism. Fluids are expelled during prograde metamorphism owing to the breakdown of hydrous phases, and these fluids can change the bulk-rock composition and thus mineralogy considerably by metasomatism. Metasomatically altered rocks are witnesses of large volumes of fluids that have interacted with a host rock and may have changed its

mineralogy, major- and trace-element chemistry, and isotope composition significantly. In turn, the newly formed minerals as well as their chemical and isotope composition can be used to constrain the origin of such metasomatic fluids and provide information on the timing of this process. An area where this allochemical metamorphism is well developed on a regional scale and can be studied in detail is the Kragerø area in the Bamble region of Southern Norway. In this area, metagabbroic and granitoid rocks were scapolitized and albitized regionally during a late stage of the Sveconorwegian orogeny at 1.06 Ga, when hydrothermal fluids infiltrated the high-grade metamorphic rocks. Similar alteration of gabbroic rocks has also been described at Modum (Munz et al.1994) and appears to be a general process that affected the Kongsberg–Bamble sectors. Pyroxene was completely replaced by amphibole, and plagioclase was either replaced by marialitic scapolite, or transformed to almost pure albite on a regional scale. Veins and pegmatites represent former fluid pathways from which the alteration was initiated and extended into the country rock. Different episodes of metasomatism are recorded by partial replacement textures and secondary mineral assemblages that require the addition of Na, Cl, Mg, Si, Al, K, P, and B to the system, whereas Fe was leached from the country rock and deposited as oxide or sulfide elsewhere (Austrheim et al. 2008; Engvik et al. 2008, 2011).

Despite these observations, the fluid history and evolution of the Bamble sector, and especially the source of the brines, have remained obscure. Possible origins include late-stage magmatic volatiles associated with the intrusion of either juvenile gabbroic dikes (Lieftink et al. 1994; Harlov et al. 2002) or granitic pegmatites (e.g., London and Kontak 2012). In contrast, Sr and Nd isotopes indicate an ancient crustal source for the albitizing fluids, which may have been generated by the breakdown of hydrous minerals within adjacent or underthrusted sediments (Munz et al. 1994). However, neither juvenile nor ancient crustal sources alone can account for the strong enrichment in Na and Mg and particularly in Cl. The addition of a seawater-derived component via either sedimentary pore fluids or evaporites mobilized during metamorphism therefore needs to be considered, as suggested by Touret (1985), Visser et al. (1999), and Engvik et al. (2011). In this study, the B and Sr isotope compositions of secondary minerals, particularly tourmaline associated with scapolite or albite, are used as tracers to identify the fluid sources.

Isotopes as tracers

Boron isotopes in tourmaline

Boron is a fluid-mobile trace element with an average abundance of ~10 μg/g in the Earth's crust. Its strong affinity for fluid phases or vapor makes it a useful tracer for hydrothermal fluids in metasomatic alteration processes (Palmer and Swihart 1996). In solution, B occurs as either trigonal $B(OH)_3$ or tetrahedral $B(OH)_4^-$ molecules, or both, depending on the pH of the fluid. Boron has two stable isotopes, ^{10}B (~20 %) and ^{11}B (~80 %), of which the lighter ^{10}B prefers the tetrahedral coordination, whereas ^{11}B favors the trigonal species (Kakihana et al. 1977). The distinct chemical behaviors of these B species result in large isotope fractionations between slightly alkaline fluids such as seawater and the solid phases interacting with or precipitating from such fluids. Seawater meets these conditions today and probably did so throughout most of Earth's history (Kasemann et al. 2010). Modern seawater has a B content of 4.6 μg/g and a $\delta^{11}B$ value of +39.6 ‰ (Foster et al. 2010), which is essentially controlled by the preferential adsorption of $^{10}B(OH)_4^-$ onto marine clay minerals, biogenic calcite, and altered oceanic crust (Schwarcz et al. 1969; Palmer et al. 1987; Hemming and Hanson 1992). This process has most likely operated since the Proterozoic, and thus, the B isotope composition of seawater has probably not changed significantly over the last ~1 Gyr. Owing to its long residence time of ~10 Myr, B is homogeneously distributed in seawater, and variations in its isotope composition depend on the interaction with other B reservoirs or changes in pH (Spivack et al. 1987).

Different geologic reservoirs show distinct B isotope signatures (Barth 1993; Marschall and Jiang 2011) with $\delta^{11}B$ ranging from −27 ‰ in non-marine evaporites (Palmer and Slack 1989) to +55 ‰ in marine brines (Vengosh et al. 1992). Mafic magmatic rocks typically contain little B (e.g., 0.5–5 μg/g), whereas substantially higher B concentrations are observed in subduction-related rocks (basaltic andesites, andesites, and rhyolites; ca. 50–500 μg/g, e.g., Clift et al. 2003; Tonarini et al. 2003; Agostini et al. 2008), and especially S-type granites. The latter may inherit large amounts of B from sediments in their sources, which may then be further concentrated through magmatic differentiation (e.g., Pesquera et al. 2013). Juvenile magmatic rocks as well as those derived from recycling average crust typically have somewhat negative $\delta^{11}B$ values around −10 ‰, whereas positive $\delta^{11}B$ values generally indicate a marine contribution, as observed in the seafloor weathering of basalts or in marine sediments. The latter represent a mixture of continental detritus (e.g., illite), authigenic marine clay (such as smectite), and carbonates, resulting in a typical range of 100–120 μg/g B with $\delta^{11}B$ between −6.6 and +4.8 ‰ for an average pelagic clay (Ishikawa and Nakamura 1993). During evaporation of seawater, $^{10}B(OH)_4^-$ is incorporated into the early precipitates of the evaporite sequence such as sulfates and carbonates, such that the residual brine becomes progressively enriched in heavy B, with $\delta^{11}B$ increasing up to +55 ‰ (Swihart et al. 1986;

Vengosh et al. 1992). Borate minerals crystallizing from such evolved brines have $\delta^{11}B$ values ranging from +11.4 to +36 ‰ (Swihart et al. 1986; Vengosh et al. 1992), which may be ascribed to the influence of interlayered clay minerals (Palmer 1991).

During prograde metamorphism, B is usually quantitatively mobilized from its host rock, transferring the distinct isotope signature of the reservoir to the emerging fluid (Palmer and Slack 1989; Palmer and Swihart 1996). If a fluid percolates through different rock types, B may be leached from various sources. Its isotope composition will then have some intermediate value, depending on B content and isotope signature of the different components. These may vary on a local scale, and regional homogenization of B isotopes within strongly folded and thrusted parts of an orogen is unlikely (Chaussidon and Albarède 1992). The contribution of ancient marine evaporites with high concentrations of isotopically heavy B will have a strong influence on the isotope signature of a hydrothermal fluid (Palmer and Slack 1989; Vengosh et al. 1992; Swihart et al. 1986; Xavier et al. 2008). Such brines may also retain other chemical features of the former evaporite such as high Na, Cl, Mg, and K contents, and may lead to the formation of scapolite and Mg-rich silicates, e.g., phlogopite, chlorite, and dravitic tourmaline (Moine et al. 1981).

Tourmaline is a chemically complex borosilicate containing 3 wt% of B. Different members of the tourmaline supergroup are typically associated with distinct chemical systems. Most form complete solid solution series, with intermediate schorl $[NaFe_3^{2+}Al_6Si_6O_{18}(BO_3)_3(OH)_3(OH)]$ to dravite $[NaMg_3Al_6Si_6O_{18}(BO_3)_3(OH)_3(OH)]$ compositions being the most common. Solid solutions between schorl and elbaite $[Na(Li_{1.5}Al_{1.5})Al_6Si_6O_{18}(BO_3)_3(OH)_3(OH)]$ are typically found in granitic pegmatites, whereas Mg-rich tourmalines may form in metasedimentary environments (Henry and Guidotti 1985). Dravite with excess Al [olenite, $NaAl_3Al_6Si_6O_{18}(BO_3)_3O_3(OH)$] and X-site vacancy [foitite component, $\square(Fe_2^{2+}Al)Al_6Si_6O_{18}(BO_3)_3(OH)_3(OH)$] is typical of medium-grade metapelitic Al-rich rocks (Henry and Dutrow 1996). However, metaevaporites and calcareous metasediments commonly contain dravite with an uvite $[CaMg_3(Al_5Mg)Si_6O_{18}(BO_3)_3(OH)_3(OH)]$ or povondraite $[NaFe_3^{3+}(Fe_4^{3+}Mg_2)Si_6O_{18}(BO_3)_3(OH)_3O]$ component, in which some Al is substituted by either Mg or Fe (Henry et al. 2008). The concentration of Ti in tourmaline coexisting with ilmenite or rutile is typically ~0.8 wt% TiO_2 (Henry and Dutrow 1996).

Prerequisites for tourmaline formation are the enrichment of B in a metamorphic or pneumatolytic fluid and the availability of corresponding major elements such as Al, Si, Mg, and Fe, which are usually host rock derived (Henry and Guidotti 1985; Henry and Dutrow 1996). Another requirement for tourmaline formation is an acidic fluid (Morgan and London 1989), in which B is dominantly trigonally coordinated. Isotope fractionation during tourmaline precipitation should then be small compared to natural variations in $\delta^{11}B$ among different reservoirs (Nakano and Nakamura 2001; Meyer et al. 2008; Marschall et al. 2009a). Once formed, the mineral is stable over a wide range of pressures and temperatures, and chemical or isotopic homogenization by volume diffusion is unlikely to occur at temperatures <600 °C (Henry and Dutrow 1996; Dutrow et al. 1999; Bebout and Nakamura 2003). Chemical and isotopic heterogeneities may thus be preserved up to at least amphibolite facies conditions, and where present, they record variable element input during tourmaline growth such as that responsible for prograde metamorphic core-to-rim zonation (Marschall et al. 2008, 2009b; Van Hinsberg et al. 2011).

Metasomatic tourmaline typically lacks strong, continuous chemical or isotopic zoning and instead shows a few wide chemical zones or a patchy element distribution pattern (Marschall et al. 2006, 2009b). Its major-element composition may be dominated by either fluid or host rock chemistry, with mixtures resulting in rare tourmaline varieties (Henry and Guidotti 1985). Some tourmaline-rich rocks originate from B-rich protoliths such as metaevaporites and contain high modes of metamorphic tourmaline (MacGregor et al. 2013). However, large crystals with high modal abundances in veins and breccias are characteristic of hydrothermal tourmalinization (Henry and Dutrow 1996). In these rocks, B is most likely derived by an external fluid infiltrating previously dehydrated basement rocks (Marschall et al. 2006, 2009b). In such cases, metasomatic tourmaline would have a B isotope composition dominated by that of the external source reservoir, but would have a major-element composition that reflects contributions from both the fluid and the replaced precursor rock. The $\delta^{11}B$ of natural tourmaline ranges from −22.8 ‰ (Palmer and Slack 1989; Klemme et al. 2011) for Broken Hill (derived from non-marine evaporites) to +28.4 ‰ in subduction zone fluids (Marschall et al. 2006), and +33.5 ‰ in dravite deposited by fluids derived from marine evaporites (Mercadier et al. 2012).

Strontium isotopes

The Sr isotope composition of Rb-poor minerals such as scapolite, apatite, and tourmaline may also be used as a tracer in hydrothermal alteration processes (King and Kerrich 1989; Mueller et al. 1991). Owing to the β^- decay of ^{87}Rb ($t_{1/2}$ = 49.76 Gyr, Nebel et al. 2011), the $^{87}Sr/^{86}Sr$ of any reservoir will strongly depend on its Rb/Sr and its age. Average continental crust has high Rb concentrations and high Rb/Sr and is thus enriched in radiogenic ^{87}Sr, with $^{87}Sr/^{86}Sr$ values typically exceeding 0.71. Rubidium is

incompatible in the depleted mantle, resulting in low Rb/Sr and low $^{87}Sr/^{86}Sr$ values of less than 0.703 in that reservoir. Strontium isotopes in seawater reflect a mixture between radiogenic Sr from continental runoff and mantle contributions at mid-ocean ridges, with typical values of ~0.709 today and ~0.705 during the Mesoproterozoic (Shields and Veizer 2002).

Minerals having a high Rb content such as mica may be used for Rb–Sr dating if they define an isochron with other Rb-bearing phases having different Rb/Sr values. However, the assumption of coeval crystallization and closure of the system is critical. In Rb-poor minerals, the Sr isotope composition will hardly change with time. For example, tourmaline that is enriched in Sr (up to 4,000 μg/g) but not in Rb (≤3 μg/g) typically has an $^{87}Rb/^{86}Sr$ of ≤0.01 (King and Kerrich 1989; Klemme et al. 2011, Marks et al. 2013). Therefore, its calculated initial $^{87}Sr/^{86}Sr$ is insensitive to age uncertainties, and should reflect the Sr isotopic composition of the source reservoir at the time of tourmaline growth. During metasomatic formation of tourmaline, Sr may be supplied by the fluid or inherited from the precursor minerals that are being replaced. A mixture of both Sr sources is likely in coupled dissolution–reprecipitation processes, as already indicated by the heterogeneous Sr isotope compositions of scapolite from the Bamble area (Engvik et al. 2011).

Geological background

The Bamble sector, southern Norway, is a 20- to 30-km-wide and 150-km-long shear belt located along the Skagerrak coastline (Fig. 1). It is bordered by the mylonitic Porsgrunn–Kristiansand shear zone to the NW and penetrated by several NE–SW-striking faults. The Mesoproterozoic basement comprises granitoid gneisses of Gothian age (~1.6 Ga) such as the Levang Granite Gneiss Dome (Rb–Sr whole-rock ages; O'Nions and Baadsgaard 1971), tonalites emplaced at 1,294 ± 38 Ma (U–Pb zircon ages; Engvik et al. 2011), and gabbroic intrusions derived from a depleted mantle source (de Haas et al. 1993, Alirezaei and Cameron 2002). The Ringsjø metagabbro yielded a U–Pb zircon age of 1,149 ± 7 Ma that was interpreted to date magmatic crystallization (Engvik et al. 2011). This age is coeval with the onset of high-grade metamorphism in this area as dated with U–Pb in primary monazite at 1,145 ± 3 Ma (Cosca et al. 1998) and 1,137 ± 1 Ma (Bingen et al. 2008a), indicating that the gabbroic intrusions may have acted as the heat source. This had already been suggested by Munz and Morvik (1991), who obtained a Sm–Nd age of 1,224 ± 15 Ma for a metagabbro in the Modum Complex, which is genetically related to the Bamble sector. The metagabbro collected across the middle part of the Bamble sector is enriched in large ion lithophile elements (LILE) and light rare earth elements (LREE) relative to normal mid-ocean ridge basalts (N-MORB), which is typical for a destructive plate margin setting (Alirezaei and Cameron 2002).

Controversial tectonic models (i.e., continent–continent collision vs. accretion) have been presented for the Sveconorwegian orogeny, but a comprehensive review is beyond the scope of this article and can be found elsewhere (e.g., Nijland et al. 2014). According to Bingen et al. (2008b), the Bamble sector developed as an accretionary wedge in an early phase of the Sveconorwegian orogeny at 1.14–1.08 Ga. Calc-alkaline to tholeiitic rocks (1.66–1.52 Ga) of the Idefjorden Terrane were subducted under magmatic rocks (1.52–1.48 Ga) and quartz-rich sediments (deposited before 1.35 Ga) of the Telemarkia Terrane. Evidence for sutures or an ophiolite sequence is absent in the Bamble area, but owing to its low K calc-alkaline signature, the 1.20–1.18 Ga gabbro–tonalite complex of Tromøy has been interpreted as a remnant of an undeveloped island arc (Smalley et al. 1983; Knudsen and Andersen 1999).

In this scenario, the metasedimentary rocks of the Bamble sector possibly originated in a shallow marine environment under (semi)arid conditions during the Mesoproterozoic (Nijland et al. 1993). This is consistent with the variety of metasediments found in the Bamble sector. Metapelitic gneisses and metagreywackes are widespread, and detrital zircon grains from quartzites yield ages of ~1.6–1.4 Ga (Åhäll et al. 1998; de Haas et al. 1999), indicating Idefjorden or Telemarkian provenance. The protoliths of intercalated lenses of orthoamphibole–cordierite gneisses may have included evaporites, as suggested by their high Mg content and highly saline fluid inclusions (Moine et al. 1981; Touret 1985). A metasomatic origin for the orthoamphibole–cordierite rocks of the Kongsberg–Bamble sectors has also been proposed (Munz 1990; Visser et al. 1994; Visser 1995; Engvik and Austrheim 2010; Hövelmann et al. 2014).

The tectonothermal reworking of the metapelitic gneisses started at 1.14 Ga (i.e., the aforementioned monazite dates), and upper amphibolite to granulite facies conditions persisted for another ~20 Myr as evidenced by metamorphic zircon ages of 1,125 ± 46 and 1,124 ± 8 Ma (Knudsen et al. 1997; Knudsen and Andersen 1999). Peak metamorphic conditions were estimated by garnet–pyroxene thermobarometry to have been 0.70 ± 0.11 GPa and 790 ± 60 °C (Harlov 2000). Subsequent cooling to below 550 °C was dated by $^{40}Ar–^{39}Ar$ in hornblende at 1,099 ± 3 and 1,079 ± 5 Ma, corresponding to cooling rates of 3–8 °C/Myr and uplift rates of 0.5–1 mm/year from crustal depths of ~30 to ~15 km (Cosca et al. 1998). During their exhumation, the high-grade metamorphic Bamble rocks were thrust onto the Telemarkia Terrane (Bingen et al.

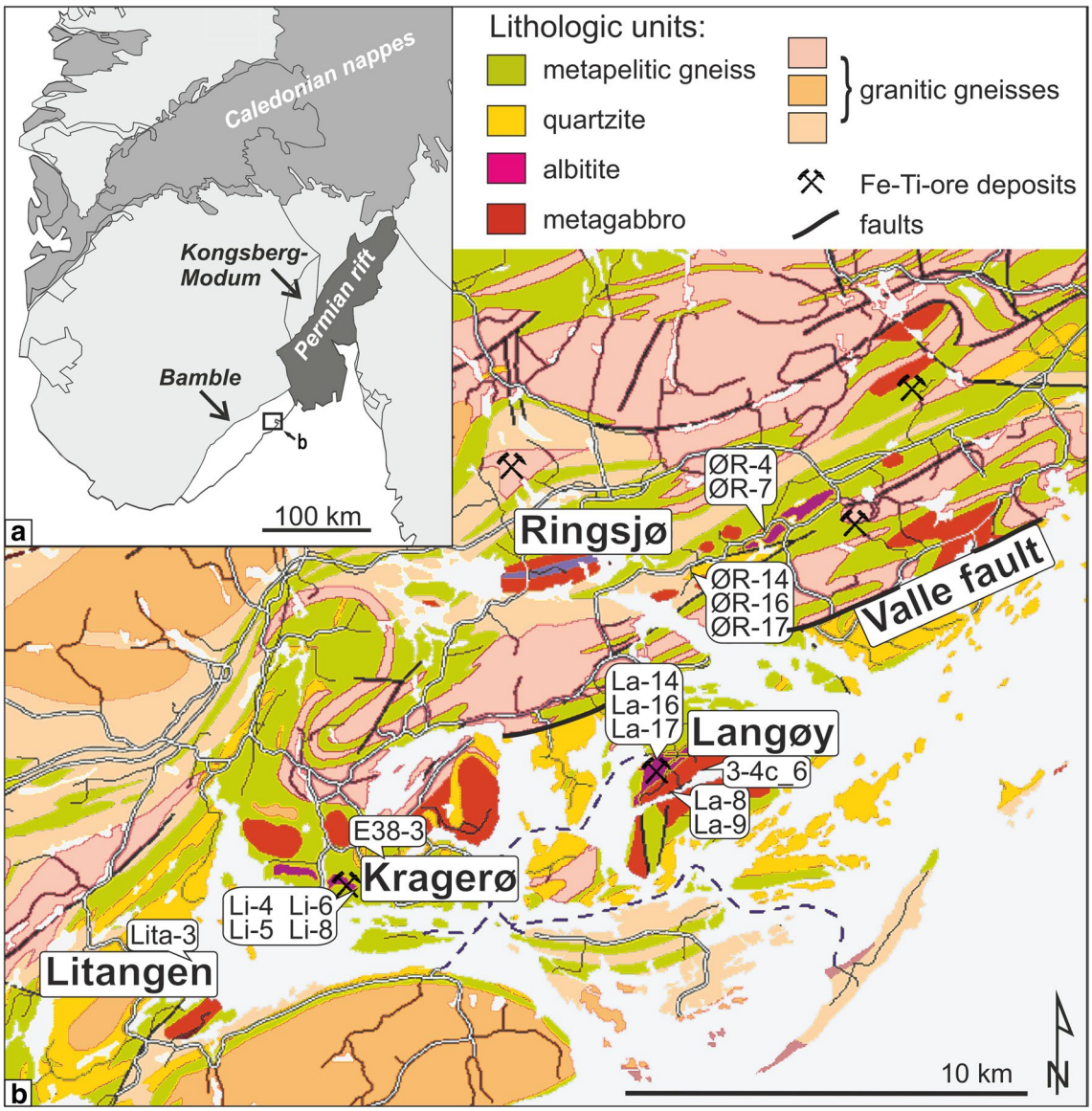

Fig. 1 **a** Overview map of southern Scandinavia pointing out the Bamble sector, from Engvik and Austrheim (2010), **b** geological map of the Bamble sector from the Norwegian Geological Survey (NGU) bedrock map database after Padget and Brekke (1996), with sample locations indicated

2008b), resulting in crustal thickening and prograde metamorphic dehydration of the Telemarkian sediments.

In the Bamble area, a subsequent period of extension was accompanied by the emplacement of granitic pegmatites at 1.06 Ga (Baadsgaard et al. 1984) and pervasive fluid infiltration along grain boundaries and fractures, resulting in abundant veining and widespread metasomatism (Engvik et al. 2011). Multiple apatite generations (Engvik et al. 2009) and replacement textures inferred from zircon coronas (Austrheim et al. 2008) record at least two stages of metasomatic alteration. The first episode was initiated by the infiltration of highly saline brines that replaced plagioclase with marialitic scapolite and F-apatite with Cl-apatite (Engvik et al. 2009). Scapolitization of the magmatic gabbro was associated with Mg metasomatism as documented by ferromagnesian minerals having high Mg contents such as phlogopite, edenitic amphibole, and dravitic tourmaline (Austrheim et al. 2008). The corresponding depletion in Fe is further recorded by the replacement of ilmenite by rutile during both scapolitization and albitization (Austrheim et al. 2008; Engvik et al. 2009, 2011). Albitization was the second pervasive alteration process and affected both the scapolite–metagabbro and granitoid rock units, producing albitite veins and pegmatite bodies. Dominated by porous albite, the typical albitite mineral assemblage comprises varying amounts of chlorite, calcite, epidote, quartz, apatite, and rutile (Engvik et al. 2008, 2009).

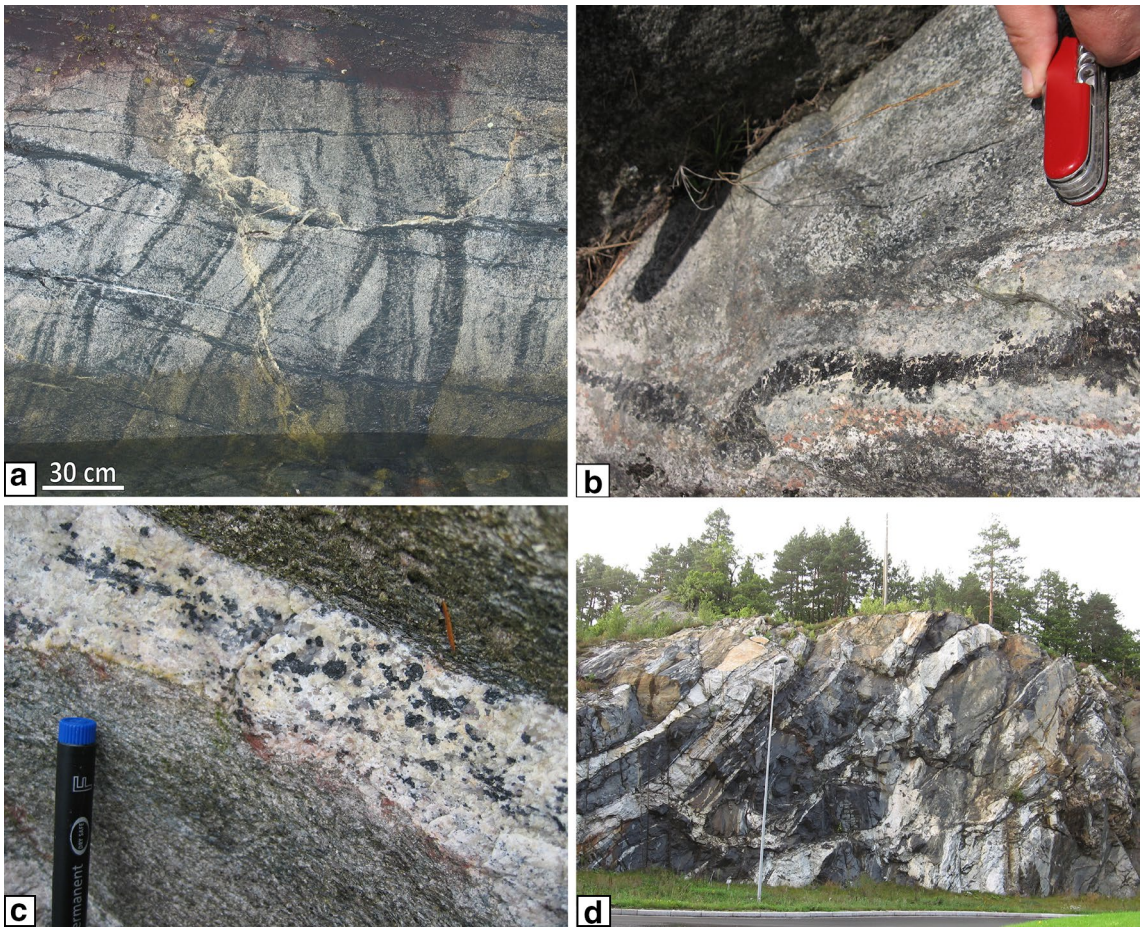

Fig. 2 Typical tourmaline occurrences associated with different alteration features: **a** scapolitized metagabbro along the shore of the island of Langøy, **b** tourmaline vein and red-stained albite in scapolitized metagabbro on the island of Langøy, **c** tourmaline-bearing albite–quartz vein crosscutting the amphibolite at Lindvikkollen, **d** heavily altered country rock along road E-38 close to Kragerø

In some places, albite appears as a dusty-looking, fine-grained alteration product that has also been sericitized, reflecting prevalent subsequent K-metasomatism. Albitites and scapolite-rich rocks are associated with Fe or Ti mineral deposits, and fine-grained hematite inclusions redden the albitized rock (Putnis et al. 2007; Engvik et al. 2008).

Sample descriptions and petrography

Different types of metasomatically altered rocks occur in the sampled localities (Fig. 1), including scapolitized metagabbro and albitite on the island of Langøy, a pegmatite in Lindvikkollen (close to Kragerø), and various metasediments. Tourmaline is typically related to veins or pegmatites, independent of the prevailing country rock (Table S1).

The island of Langøy

The metagabbro on the island of Langøy (Fig. 2a), an important source of iron ore in the past, is pervasively scapolitized and crosscut by tourmaline-bearing veins (Fig. 2b) that comprise varying amounts of albite, epidote, and calcite (Fig. 3a, b) as well as minor amounts of chlorite, biotite, and Fe oxides or sulfides. Tourmaline crystals are coarse-grained and euhedral (Fig. 3c, d) but cracked, with the fractures typically being filled with other minerals of the albitite assemblage. The influence of Na metasomatism is restricted to the realm of the vein, where albite is abundant and mafic phases have been chloritized. Scapolitization penetrated more deeply into the rock, replacing the metagabbro with a fine-grained mineral assemblage of amphibole and scapolite. Phlogopite and Fe oxides formed at the expense of ilmenite. Within the best-preserved parts, the metagabbro still exhibits a subophitic texture (Fig. 3, right-hand side). At ca. 10 cm from the vein, the onset of scapolitization is documented by remnant plagioclase, which has been partially replaced and blackened by inclusions of spinel (Fig. 3g, h). Small tourmaline crystals (1.5 mm diameter, sample La-8_small, Fig. 3i, j) are color zoned, with a gradation from blue–green cores to brown rims.

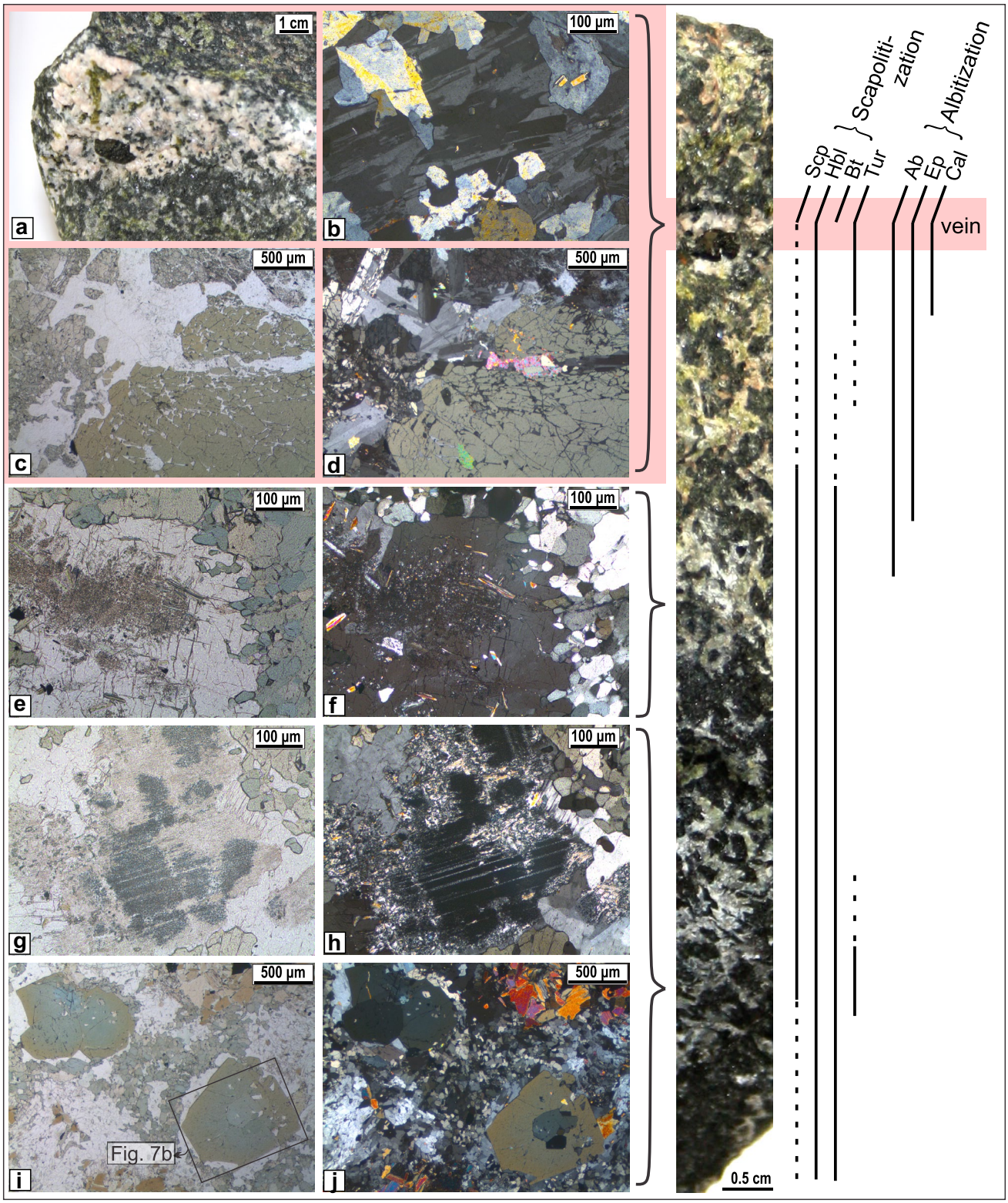

Fig. 3 Photographs, and plane- and cross-polarized light photomicrographs showing the different alteration stages recorded in sample La-8: **a** tourmaline in sample La-8 situated at the albitized vein, **b** cross-polarized light image of the epidote-bearing albite vein, **c**, **d** fractured tourmaline and amphibole within the vein, **e**, **f** scapolitized metagabbro, **g**, **h** partly scapolitized plagioclase with preserved twinning, blackened by spinel, **i**, **j** small tourmaline crystals (sample La-8_small) in scapolitized metagabbro

The albitized vein samples, La-16 and La-17, were found on the western part of the island, where a Fe oxide-bearing albitite breccia (sample La-14) crosscuts the scapolitized metagabbro. This coarse-grained rock is dominated by porous albite, which is in places sericitized along cleavage planes, and also contains quartz, tourmaline, calcite, white mica, and accessory biotite and zircon. Zoned tourmaline crystals with blue cores and brown rims are crosscut by brownish tourmaline veins and have inclusions of euhedral albite.

Kragerø area

The country rock at Lindvikkollen in the vicinity of Kragerø is a banded amphibolite that comprises clusters of green amphibole in a matrix of biotite and plagioclase, which is in some places strongly sericitized. Within this very fine-grained alteration product, a 0.8-cm diameter euhedral tourmaline crystal occurs in apparent equilibrium with albite and hematite (sample Li-5). The amphibolite is cut by numerous tourmaline-bearing, quartz–albite–K-feldspar veins (samples Li-4 and Li-6, Fig. 2c). As summarized by Larsen (2008), the amphibolite at Lindvikkollen hosts a granite–pegmatite described early on by Brøgger (1906). The pegmatite consists mostly of quartz and reddened microcline, and is known as a rutile deposit (Korneliussen and Furuhaug 2000). In sample Li-8, a network of tourmaline veinlets containing a few inclusions of quartz extends into a large crystal of pink-stained microcline. The 7.5-cm-long black tourmaline crystal is fractured and displays a macroscopically visible vein network and inclusions of chlorite.

Extensively tourmalinized metasediments were also found north of Lindvikkollen along road E38 (Kragerøveien). Partly migmatized and deformed metasediments are strongly altered and interlayered with granitic pegmatites (Fig. 2d, sample E38-3). The tourmaline crystals from this area are typically fractured perpendicular to the *c*-axis and crisscrossed by calcite–apatite veins that contain minor Fe sulfides and oxides.

Litangen quartzite quarry

The Kragerø domain comprises massive quartzites that are commercially exploited at Litangen (sample Lita-3). In the Litangen quartzite quarry, up to 5-cm-long crystals of tourmaline and quartz occur together with sillimanite and several types of mica. In sample Lita-3, white mica, rutile, and zircon occur as inclusions in both tourmaline and quartz. The outer parts of the tourmaline crystals were mechanically broken, and the fractures were filled with quartz, white mica, and zircon. Quartz recrystallized to large, unfractured grains, and is either pure white or, in other places, reddened by hematite, indicating the mobility of Fe during hydrothermal alteration.

Ødegården–Ringsjø area

The mylonitic Valle Fault delimits these distinct metasedimetary units to the NW and separates the Kragerø domain from the adjacent Ringsjø area (Padget 2004), where tourmaline was found in strongly albitized rock units related to Mg–Al-rich metasediments (samples ØR-4, ØR-7, ØR-14, ØR-15, ØR-19).

Two localities were sampled north of the Valle fault along the Frosteveien in the Ødegården-Ringsjø area. A strongly altered rock (sample ØR-4) was found along an albitization front in a transect that merges into a tourmaline-bearing orthoamphibole–cordierite gneiss (sample ØR-7). The large tourmaline crystals of sample ØR-4 are altered along grain boundaries and contain calcite inclusions. In some places, a sharp replacement front is visible. The albite is porous and in some places strongly sericitized. Biotite has inclusions of zircon, and amphibole has been altered to chlorite.

An albitite containing tourmaline in veins as well as single crystals ranging from a few mm in diameter (sample ØR-15) up to several cm (sample ØR-14) was also sampled. In thin section, the larger (>1 cm) crystals typically display a patchy optical zonation and are related to fine-grained alteration products of albitization. Small (~1 mm) tourmaline crystals typically occur in clusters together with quartz. Albite and K-feldspar are both strongly altered, and the albitization seems to have been coupled to hematite precipitation resulting in reddening of the rock. The albitite also contains quartz, apatite, white mica, and scapolite, with accessory opaque Fe oxides, ilmenite, and rutile.

Methods

In situ analyses of major elements and B isotopes

The major-element chemistry of tourmaline was analyzed with an electron microprobe (JEOL JXA 8900 Superprobe, Institut für Mineralogie, Westfälische Wilhelms-Universität Münster) equipped with four wavelength-dispersive spectrometers (WDS). The B isotope compositions were measured with an ion microprobe (Cameca ims 3f) at the Institut für Geowissenschaften, Universität Heidelberg. Analyses were performed on thin sections and grain mounts consisting of several tourmaline crystals embedded in epoxy.

For electron probe microanalyses (EPMA), a beam current of 15 nA and an accelerating voltage of 15 kV were used. Counting times of 5 s were applied for the volatile alkali metals and halogens and 10 s for all other elements, with interposed background measurements lasting 2.5

and 5 s, respectively. Detection limits were generally better than 200 μg/g. The relative standard deviation (1σ) on reported values is typically <3 % for most elements, except for Ti with 1σ <5 %. The φ(ρZ) correction method of Armstrong (1988, 1991) was used for data reduction. Tourmaline compositions were calculated assuming 31 O atoms per formula unit (apfu) and stoichiometric amounts of B (3 apfu) as suggested by Henry and Guidotti (1985).

For element mapping, Na, Mg, Si, and Al were determined with an energy-dispersive spectrometer (EDS), whereas B, Ca, Fe, and Ti were measured by WDS. Again, an accelerating voltage of 15 kV was applied. However, the beam current was raised to 50 nA to reduce counting times to 150–250 ms per spot while still getting acceptable count rates. The electron beam was defocused to 5 or 10 μm to cover a larger area with no space between adjacent spots.

For the B isotope determinations in tourmaline by secondary ion mass spectrometry (SIMS), the analytical protocol of Marschall et al. (2009a) was used. The O^- primary ion beam was accelerated to 14.5 keV at a beam current of 1 nA. The diameter of the spot used for sputtering was 5–10 μm. To remove surface contamination and to reach steady-state conditions, spots were presputtered for 4 min before the actual analysis started. The energy window was adjusted to 100 eV, and no energy offset was applied. Molecular interferences (e.g., ^{9}BeH, ^{10}BH, and $^{30}Si^{3+}$) were sufficiently resolved by using a mass resolution of ~1,200. Secondary B^+ ions were separated by a double-focusing mass spectrometer and were detected by a single electron multiplier in pulse-counting mode. The settling time between the two different masses was 200 ms. Each $^{11}B/^{10}B$ measurement consists of 50 ^{10}B–^{11}B–^{10}B cycles, with integration times of 2 × 1.66 s for ^{10}B and 1.66 s for ^{11}B and typical count rates of ~5×10^4 s^{-1} (^{10}B) and ~2×10^5 s^{-1} (^{11}B). The total analysis time was ~10 min for each spot. Three different reference tourmalines (98114 elbaite, 108796 dravite, and 112566 schorl; Dyar et al. 2001; Leeman and Tonarini 2001) were used to determine the instrumental mass fractionation α_{inst}. For a detailed description of the analytical setup, see Ludwig et al. (2011). The reference materials were analyzed before, during, and after the measurement session, resulting in a mean α_{inst} of 0.9571 ± 0.0006 (1σ) for the first and 0.9564 ± 0.0008 (1σ) for the second analytical session. The internal precision of a single analysis was better than 0.5 ‰ (1σ), with an external reproducibility of ±0.5 ‰ (1σ). Boron isotope ratios are reported in δ-notation ($\delta^{11}B$) as per mil deviation relative to the NIST boric acid standard SRM-951 as reported by Catanzaro et al. (1970). To check for correlations between $\delta^{11}B$ and bulk composition during multi-spot traverses of zoned tourmaline, the secondary ion intensity of $^{56}Fe^+$ was recorded manually after some of the B isotope analyses.

Rb–Sr analyses

Selected rock samples were crushed with a steel mortar and sieved. After pre-concentration with a Frantz® magnetic barrier separator, mineral separates from the >250 μm fraction were prepared by handpicking inclusion-free grains under a binocular microscope. For plagioclase, scapolite, biotite, amphibole, epidote, tourmaline, and whole-rock fractions, aliquots of 10–50 mg were weighed into Savillex® Teflon® vials. A mixed ^{87}Rb–^{84}Sr tracer was then added before dissolving the sample in distilled acids ($HF:HNO_3 = 5:1$) at 120 °C for 48 h. Afterwards, the samples were dried down on a hot plate at 120 °C. In contrast, tourmaline and whole-rock samples were decomposed in $HF:HNO_3$ (5:1) under pressure in Savillex® vials placed in Parr® bombs at 180 °C for 5 days and then dried down with $HClO_4$ to break down fluorides. Residues from both types of digestion were then dissolved in 6 M HCl, dried down, taken up in 2.5 M HCl, and centrifuged for 10 min. Rubidium and Sr were separated by cation exchange chemistry in quartz columns filled with Bio-Rad AG 50W-X8 resin, 200–400 mesh. After the Rb cut was separated, the Sr-bearing cut was processed through the column chemistry once again to remove any remaining Rb. Maximum procedural blanks were 21 pg Sr and 6 pg Rb.

Isotope analyses were carried out by multi-collector thermal ionization mass spectrometry (MC-TIMS) at the Institut für Mineralogie, Westfälische Wilhelms-Universität Münster. Strontium isotope ratios were measured on a Finnigan Triton, whereas Rb was measured on a VG Sector 54. Replicate analyses of the NIST standards SRM-987 (Sr) and SRM-607 (Rb) yielded mean values of $^{87}Sr/^{86}Sr = 0.710120 \pm 9$ and $^{87}Rb/^{85}Rb = 0.3844 \pm 63$ (2 s.d.), which is within error of the certified values. The estimated external reproducibilities based on repeated measurements of spiked samples and standards (2 s.d.) are 0.004 % for $^{87}Sr/^{86}Sr$ and 1 % for $^{87}Rb/^{86}Sr$. The initial $^{87}Sr/^{86}Sr$ values were calculated using $\lambda^{87}Rb = 1.393 \times 10^{-11}$ $year^{-1}$ (Nebel et al. 2011) and an estimated age of 1,060 Ma (Engvik et al. 2011).

Results

Tourmaline major-element chemistry

The tourmaline compositions as determined by EPMA are summarized in Table 1 and classified according to their principal *X*- and *Y* + *Z*-site occupancy (Henry et al. 2011) in Fig. 4. Although chemically diverse, all investigated tourmaline samples are Na-dominated on the *X*-site and thus belong to the alkali group (Fig. 4a). They show minor Ca components or *X*-site vacancies (□) that correlate with Al

contents of 5–7 apfu, indicating an additional uvite or foitite component. The ternary Al–Fe–Mg-diagram (Fig. 4b) was proposed by Henry and Guidotti (1985) to classify tourmaline according to different genetic environments. However, newly crystallized, metasomatic tourmaline may inherit chemical and isotopic characteristics of both precursor rock and fluid, and may thus display a composition that does not correspond to a single environment. Furthermore, hydrothermal tourmaline associated with metaevaporites may define a trend between "oxy-dravite" and povondraite (dotted line in Fig. 4b) as described by Henry et al. (2008). Most of the investigated tourmalines roughly follow this trend. Only samples Li-6, La-14, ØR-14, and ØR-15 are rather Fe-rich, with X_{Mg} (= Mg/[Fe^{2+}+Mg]) <0.3 and plot in fields 1, 2, and 3.

Tourmaline samples from Langøy are sodic with Ca contents between 0.1 and 0.3 apfu and no significant *X*-site vacancy. Tourmaline associated with the scapolitized metagabbro is typically dravitic ($X_{Mg} > 0.6$) with an uvite component that is minor in samples 3–4c_6, La-8, and La-9, but more significant in samples La-16 and La-17, which have an Al content of ~5 apfu. Tourmaline associated with the Langøy metagabbro is significantly enriched in Ti, with contents up to 0.24 apfu, except for sample La-14, which is a somewhat heterogeneous schorl ($X_{Mg} = 0.3$) with low Ti content (0.04 apfu).

Tourmaline from Lindvikkollen is generally sodic to calcic with little to no X-site vacancy. With $X_{Mg} = 0.15$, sample Li-6 contains homogeneous schorl such as that typically found in granitic pegmatites. Although sampled within 100 m of Li-6, samples Li-4 and Li-5 are dravitic tourmaline with $X_{Mg} > 0.6$ that contain an uvite component with Ca contents up to 0.3 apfu and Al $\leq$ 5 apfu. The tourmalines from Li-4 and Li-5 have similar chemical compositions, although they come from different lithological units (albitite and amphibolite, respectively). The chemically heterogeneous tourmaline in sample Li-8 plots along the "oxy-dravite"-povondraite trend.

Tourmalines in samples E38-3 and Lita-3 are chemically similar, although found at different localities in distinct lithological units (tourmalinized metasediments including quartzite). Both are slightly heterogeneous dravite with $X_{Mg} > 0.8$ and Ca contents up to 0.3 apfu. The *X*-site vacancies of 0.2 apfu and excess Al up to 6.5 apfu indicate an additional foitite component, which is common for tourmaline in medium- to high-grade metapelites. For sample E38-3, element mapping by EPMA revealed pseudomorphic replacement features recorded by an intricate chemical zonation reminiscent of hierarchical reactive fracture formation in other minerals (Fig. 5).

Tourmalines associated with the orthoamphibole–cordierite rocks in Ringsjø (samples ØR-4 and ØR-7) are dravitic with X_{Mg} between 0.60 and 0.75. Sample ØR-4 contains a significant uvite component (0.4 apfu Ca), which is typical for tourmaline associated with calcareous metasediments. However, no remnants of such sediments were found in the field, so the tourmaline-forming fluids may derive from a different type of source rock. The tourmaline crystal is further enriched in Ti with 0.22 apfu and has a Ca–Ti-poor alteration zone with some additional overgrowth. The major-element chemistry of sample ØR-7 is similar to this secondary tourmaline rim.

Samples from the albitite pegmatite in Ringsjø contain chemically heterogeneous tourmaline with variable X_{Mg} ranging from ~0.2 to ~0.4 (ØR-14 and ØR-15), or ~0.6 (ØR-19). Significant foitite components are displayed by *X*-site vacancies up to 0.25 and excess Al up to 7.5 apfu (ØR 15).

Boron isotopes in tourmaline

The measured ranges in $\delta^{11}B$ values for each sample are given in Table 2. The results are compared to typical isotope signatures of possible B source reservoirs (Fig. 6). The B isotope signatures vary throughout the studied field area, with an overall spread in $\delta^{11}B$ values of 33 ‰, ranging from −5.6 to +27.4 ‰. The lowest $\delta^{11}B$ values are observed for tourmaline from Lindvikkollen with $\delta^{11}B$ as low as −5.6 ‰ (sample Li-6). The $\delta^{11}B$ of Li-5 is as low as −4.8 ‰, whereas Li-4, sampled some hundred meters away, has less negative $\delta^{11}B$ values of −3.1 to −1.9 ‰. Sample Li-8, which was collected from the mine tailings, has more positive and variable $\delta^{11}B$ values ranging from −0.4 to +3.7 ‰, with no obvious correlation to major-element abundances. Boron isotope signatures within a similar range are observed for tourmalinized sediments found in the vicinity of Kragerø (sample E38-3). Although this tourmaline is heterogeneous with respect to its major-element composition (Fig. 5), its $\delta^{11}B$ ranges only from +1 to +2.4 ‰. Tourmaline related to the Litangen quartzite (Lita-3) has $\delta^{11}B$ values that overlap with those from Lindvikkollen, but are generally more positive and range from +1.3 to +6.6 ‰.

Tourmalines from the island of Langøy have $\delta^{11}B$ values that cluster around 0 to +3 ‰. However, tourmaline samples such as La-8_small, La-14, and La-17 are somewhat different, showing a larger spread in $\delta^{11}B$ from −2.5 to +8.4 ‰, −1.9 to +4.2 ‰, and from −3.2 to +2.3 ‰, respectively. For the small tourmaline crystals of sample La-8, a negative correlation between their $\delta^{11}B$ values and their Ti contents is observed (Fig. 7). Furthermore, the B isotope signature and Ti content of the rim are similar to those of the large tourmaline sampled along the vein in La-8 (Fig. 3). The variations in sample La-14 are attributed to different generations of tourmaline as identified by the Fe distribution (Fig. 8a). In accordance with other

Table 1 Tourmaline major-element chemistry; B is calculated stoichiometrically as three apfu

wt %	Li-4	Li-5	Li-6	Li-8	Lita-3	E38-3	3-4c_6	La-8 vein	La-8* core	La-8* rim	La-9
B_2O_3	10.21	10.25	9.98	10.08	10.63	10.77	10.54	10.44	10.62	10.49	10.49
SiO_2	35.85	35.99	33.91	35.36	35.75	36.92	36.22	35.79	36.53	36.05	36.34
Al_2O_3	24.69	24.30	28.14	24.30	32.94	32.10	29.51	28.92	29.88	28.91	28.41
TiO_2	1.10	1.24	0.45	0.96	0.51	0.73	0.93	1.08	0.33	0.99	1.28
FeO	8.97	10.59	19.24	15.56	3.61	3.03	4.85	6.83	6.58	6.85	5.99
MgO	10.32	9.93	1.98	6.79	8.54	9.51	9.73	8.84	9.14	9.13	9.28
CaO	1.76	1.91	0.59	1.66	1.80	1.46	1.21	1.46	1.44	1.31	0.95
Na_2O	2.01	1.90	2.47	1.98	1.50	1.73	2.54	2.32	2.46	2.35	2.61
K_2O	0.05	0.06	0.10	0.07	0.07	0.03	0.03	0.02	0.01	0.04	0.03
Σ wt %	95.06	96.32	97.20	96.85	95.46	96.45	95.57	95.87	96.98	96.11	95.91
Apfu											
B	3.00	3.00	3.00	3.00	3.00	3.00	3.00	3.00	3.00	3.00	3.00
Si	6.10	6.10	5.91	6.10	5.85	5.96	5.98	5.95	5.98	5.97	6.02
Al_T	0.00	0.00	0.00	0.00	0.15	0.04	0.00	0.00	0.00	0.00	0.00
Al_Z	4.95	4.85	5.77	4.94	6.00	6.00	5.74	5.67	5.76	5.64	5.55
Al_Y	0.00	0.00	0.00	0.00	0.35	0.10	0.00	0.00	0.00	0.00	0.00
Ti	0.14	0.16	0.06	0.12	0.06	0.09	0.12	0.14	0.04	0.12	0.16
Fe	1.28	1.50	2.80	2.25	0.49	0.41	0.67	0.95	0.90	0.95	0.83
Mg	2.62	2.51	0.51	1.75	2.08	2.29	2.39	2.19	2.23	2.25	2.29
Y total	4.05	4.19	3.43	4.13	3.00	2.91	3.20	3.30	3.20	3.35	3.35
Ca	0.32	0.35	0.11	0.31	0.32	0.25	0.21	0.26	0.25	0.23	0.17
Na	0.66	0.62	0.84	0.66	0.47	0.54	0.81	0.75	0.78	0.75	0.84
K	0.01	0.01	0.02	0.02	0.01	0.01	0.01	0.00	0.00	0.01	0.01
X total	1.00	0.98	0.97	0.99	0.80	0.80	1.03	1.01	1.04	0.99	1.01
F	0.03	0.00	0.00	0.02	0.00	0.00	0.00	0.00	0.00	0.00	0.00
Cl	0.01	0.01	0.01	0.01	0.01	0.00	0.07	0.00	0.02	0.01	0.01
X_{Mg}	0.67	0.63	0.15	0.45	0.81	0.85	0.78	0.70	0.71	0.70	0.73
n	3	21	3	110	57	6	18	13	4	3	4

wt %	La-14	La-14[#]	La-16	La-17	ØR-4	ØR-4[†]	ØR-7	ØR-14	ØR-15	ØR-15[‡]	ØR-19
B_2O_3	10.10	10.66	10.20	10.28	10.33	10.35	10.61	10.32	10.55	10.60	10.53
SiO_2	33.84	36.77	35.50	35.93	35.52	36.10	36.50	34.71	34.20	35.53	35.78
Al_2O_3	29.55	29.28	24.84	25.11	26.38	28.82	31.03	32.04	36.82	33.70	31.88
TiO_2	0.31	0.56	1.89	1.84	1.74	0.07	0.58	0.22	0.36	0.49	0.55
FeO	15.35	8.28	9.95	10.48	9.20	9.42	5.28	14.49	11.73	8.89	8.11
MgO	3.67	7.56	8.99	8.94	9.04	7.87	8.76	2.59	1.45	5.13	6.50
CaO	0.53	0.76	1.79	1.27	2.23	0.60	0.66	0.60	0.32	0.64	0.95
Na_2O	2.71	2.38	2.10	2.34	1.74	2.47	2.47	2.31	2.12	2.20	2.10
K_2O	0.08	0.03	0.05	0.03	0.08	0.02	0.01	0.08	0.10	0.07	0.07
Σ wt %	96.68	98.55	95.55	96.41	96.33	95.77	95.91	97.46	88.99	89.10	96.54
Apfu											
B	3.00	3.00	3.00	3.00	3.00	3.00	3.00	3.00	3.00	3.00	3.00
Si	5.82	6.00	6.05	6.07	5.97	6.06	5.98	5.85	5.63	5.83	5.91
Al_T	0.07	0.00	0.00	0.00	0.00	0.00	0.00	0.15	0.37	0.17	0.08
Al_Z	5.89	5.63	4.99	5.00	5.23	5.70	5.98	5.98	6.00	6.00	5.96
Al_Y	0.10	0.00	0.00	0.00	0.00	0.00	0.01	0.38	1.15	0.51	0.25
Ti	0.04	0.07	0.24	0.23	0.22	0.01	0.07	0.03	0.04	0.06	0.07
Fe	2.21	1.13	1.42	1.48	1.29	1.33	0.72	2.04	1.62	1.22	1.12
Mg	0.94	1.84	2.28	2.25	2.27	1.97	2.14	0.65	0.36	1.26	1.60
Y total	3.37	3.33	3.98	3.99	3.79	3.31	2.97	3.11	3.20	3.06	3.05

Table 1 continued

wt %	La-14	La-14#	La-16	La-17	ØR-4	ØR-4†	ØR-7	ØR-14	ØR-15	ØR-15‡	ØR-19
Ca	0.10	0.13	0.33	0.23	0.40	0.11	0.12	0.11	0.06	0.11	0.17
Na	0.90	0.75	0.69	0.77	0.57	0.80	0.78	0.75	0.68	0.70	0.67
K	0.02	0.01	0.01	0.01	0.02	0.00	0.00	0.02	0.02	0.01	0.01
X total	1.02	0.89	1.03	1.00	0.99	0.92	0.90	0.88	0.75	0.82	0.85
F	0.00	0.11	0.00	0.00	0.00	0.00	0.00	0.00	0.00	0.00	0.00
Cl	0.01	0.00	0.01	0.01	0.02	0.03	0.01	0.02	0.01	0.01	0.01
X_{Mg}	0.30	0.62	0.62	0.60	0.64	0.60	0.75	0.24	0.18	0.50	0.59
n	17	1	14	23	32	9	16	21	13	9	24

* Small (1.5 mm diameter) tourmaline crystal in sample La-8

Tourmaline veins in sample La-14

† Overgrowth in sample ØR-4

‡ Fe-poor growth zone in tourmaline ØR-15

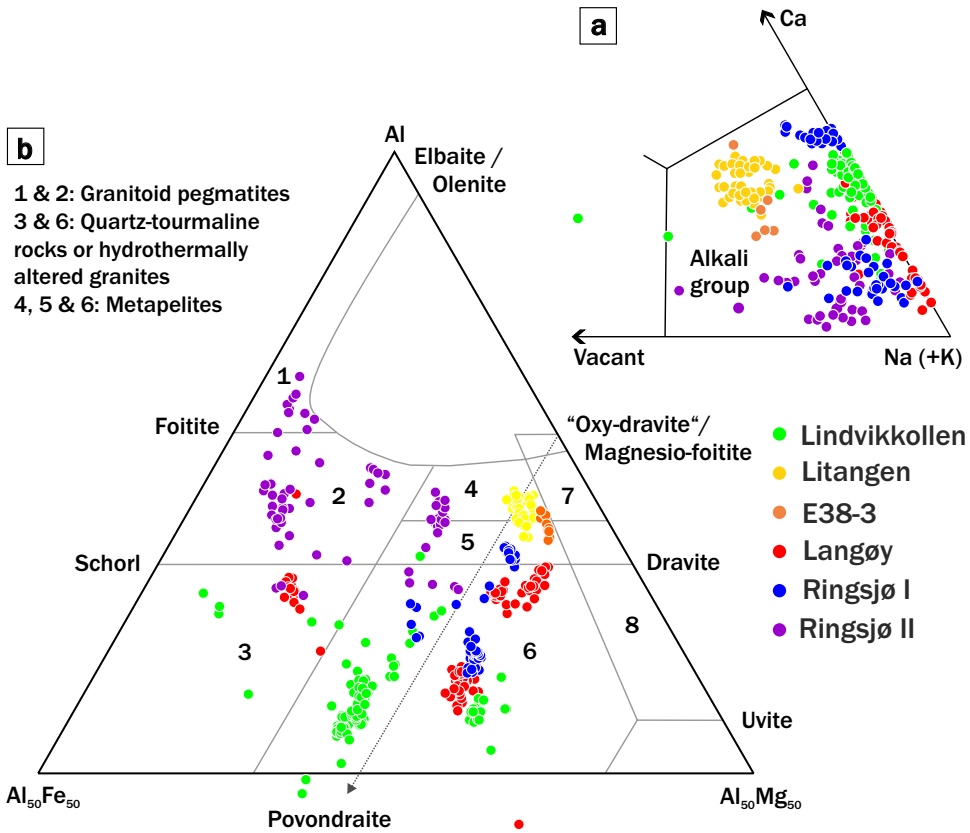

Fig. 4 Tourmaline major-element chemistry, data are sorted by tourmaline sample location; most samples roughly follow the "Oxy-dravite"-Povondraite trend (across fields 4, 5, 6), whereas a few others (ØR-14, ØR-15, La-14, Li-6) are rather Fe-rich (fields 2, 3)

tourmaline samples from Langøy, the first tourmaline generation of La-14 has $\delta^{11}B$ values around +3 ‰ (Fig. 8b). However, the isotopic compositions of the later, Fe-poor tourmaline veins cluster around -1 ‰ and are thus significantly different.

Large tourmaline crystals from Ringsjø have fairly homogeneous B isotope signatures ranging from +4.8 to +6.2 ‰ in sample ØR-14 and from +3.8 to +5.9 ‰ in sample ØR-19. However, a small tourmaline crystal from the same outcrop (ØR-15) shows a larger spread in $\delta^{11}B$, ranging from +3.5 to +9.5 ‰. Again, the variability can be attributed to different generations of tourmaline (Fig. 8c), and Fe contents correlate with B isotopes in the Fe-poor growth zone (Fig. 8d).

The isotopically heaviest B with $\delta^{11}B$ up to +27.4 ‰ was detected in tourmaline from Ringsjø (ØR-4) that was found close to an orthoamphibole–cordierite gneiss. This 8-mm-diameter tourmaline crystal has a Ca–Ti-poor growth zone at its rim, where $\delta^{11}B$ values decrease to +18 ‰ (Fig. 9). However, tourmaline directly associated with orthoamphibole and cordierite (sample ØR-7) has less positive $\delta^{11}B$ signatures between +7.3 and +10.7 ‰.

Strontium isotopes

The measured Rb and Sr concentrations and $^{87}Sr/^{86}Sr$, as well as the calculated initial $^{87}Sr/^{86}Sr$ values are given in Table 3 for all rocks and minerals analyzed. Linear

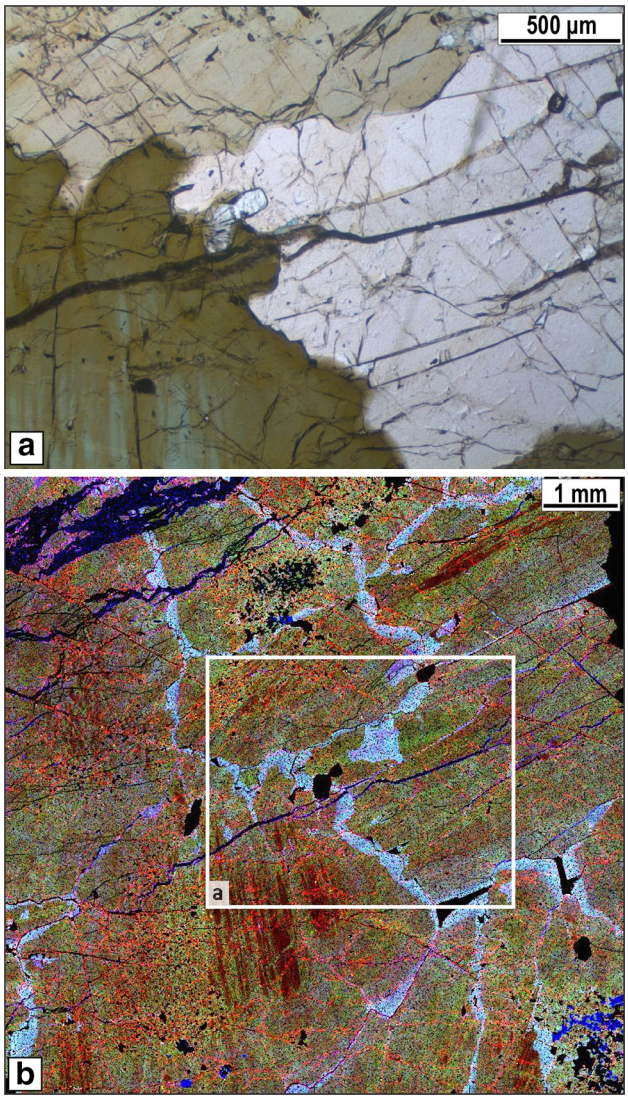

Fig. 5 **a** Thin section image of sample E38-3, and **b** composite element map (red = Fe, green = Ti, blue = Ca) showing pseudomorphic tourmalinization; single-element maps for B, Fe, Ca, and Ti can be found in Fig. S1 in the electronic supplementary material

regressions for mica and the Rb-poor minerals scapolite, amphibole, tourmaline, epidote, and feldspar were constructed for each sample using Isoplot (Ludwig 2009). The resulting Rb–Sr dates (utilizing all phases analyzed) are 1,062 ± 23 Ma (Li-5), 1,068 ± 10 Ma (Lita-3), 1,070 ± 15 Ma (ØR-4), 1,051 ± 12 Ma (La-8), and 1,043 ± 16 Ma (ØR-19/20). The slopes of these isochrons are mainly defined by mica ($^{87}Rb/^{86}Sr > 55$); thus, the dates obtained from the regressions potentially reflect the metasomatic formation ages of the mica or their cooling below the closure temperature for the Rb–Sr system. Large scatter among the low Rb/Sr minerals results in high MSWD values (≥64), indicating that inherited (precursor) minerals were only partially equilibrated during metasomatism or their Rb–Sr systems closed at slightly different times. As a result, individual minerals of each sample reveal highly variable initial $^{87}Sr/^{86}Sr$ values calculated for an estimated age of 1,060 Ma. Unrealistic values below 0.69898 (i.e., BABI, basaltic achondrite best initial; Papanastassiou and Wasserburg 1969) are due to differing Sr evolution of the individual minerals used in the regression and lack of isotopic homogenization at 1,060 Ma. Despite these effects, two-point isochrons between mica and the whole rock or any one of the low Rb/Sr phases yield consistent dates within and between rock samples, suggesting that metasomatic mica crystallization indeed occurred at ca. 1.07–1.04 Ga, in agreement with Engvik et al. (2011).

Discussion

Different alteration stages

Late-stage orogenic hydrothermal alteration processes in the Kragerø area can be subdivided into several metasomatic stages related to different fluid pulses. Initially, brines rich in Na, Cl, Mg, K, P, and B caused pervasive amphibolitization and scapolitization of gabbros and other precursor rocks (Austrheim et al. 2008; Engvik et al. 2011; Kusebauch et al. 2014). Biotite also formed early in the metasomatic alteration history, when K was still available, and incorporated Ti, which was mobilized by the brine. This metasomatic biotite is commonly easily recognizable by its distinct reddish color typical for phlogopite-rich biotite. Simultaneously, Ti-poor tourmaline (cores of sample La-8 small) formed. These first tourmaline crystals have positive $\delta^{11}B$ values up to +8.4 ‰. Subsequently grown rims as well as the large tourmaline crystal sampled along the vein in sample La-8 have higher Ti contents and less positive $\delta^{11}B$ values around +3 ‰. The initial Sr isotope compositions of tourmaline and amphibole are in the same range (ca. 0.703, Table 3) and suggest that these minerals formed at the same time from the same reservoir. The signature reflects mantle-derived Sr, which may have been inherited from the gabbroic precursor during the first alteration stage, i.e., scapolitization. In contrast, epidote is clearly enriched in radiogenic Sr ($^{87}Sr/^{86}Sr = 0.706$, Table 3), which may have been derived by the crustal fluid that caused albitization. This secondary alteration stage is documented by varying amounts of albite, epidote-group minerals, calcite, and chlorite. Veins that acted as fluid pathways recrystallized to this albitite mineral assemblage (e.g., sample La-8, Fig. 3). Here, secondary tourmaline did not form during the albitization, suggesting that insufficient B was available or that tourmaline was not stable in the fluid. Instead, euhedral tourmaline crystals found along those veins were apparently broken mechanically by hydrostatic pressure of the

Table 2 Summary of the Boron isotope compositions of tourmaline; all measured data can be found in Table S2 in the electronic supplementary material

Sample	$\delta^{11}B_{low}$	s.d.	$\delta^{11}B_{high}$	s.d.	$\delta^{11}B_{mean}$	s.d.	*N*
Lindvikkollen							
Li-4	−3.1	0.9	−1.9	1.0	−2.6	0.5	4
Li-5	−4.8	1.1	−3.4	0.9	−4.2	0.5	5
Li-6	−5.6	0.8	−3.5	0.8	−4.6	0.8	7
Li-8	−0.4	0.7	+3.6	0.8	+1.3	1.1	20
Litangen							
Lita-3	+1.3	0.9	+6.6	0.7	+2.6	1.2	42
Kragerø							
E38-3	+1.0	0.9	+2.4	0.8	+1.8	0.6	5
Langøy							
La-8	+2.2	0.8	+3.2	1.0	+2.7	0.4	4
La-8 small	−2.5	1.0	+8.4	0.9	+4.6	2.8	29
La-9	+1.5	0.8	+3.8	0.9	+2.7	1.0	5
La-14	−1.9	0.7	+4.2	0.8	+2.0	1.9	25
La-16	+2.4	0.7	+3.7	0.9	+3.3	0.6	4
La-17	−3.2	0.8	+2.3	0.8	+0.5	1.6	12
3-4c_6	−0.9	0.9	+1.4	0.8	+0.3	0.6	14
Ødegården/Ringjø							
ØR-4	+16.5	0.8	+27.4	0.7	+23.4	3.2	32
ØR-7	+7.3	0.8	+10.7	0.8	+8.2	0.9	19
ØR-14	+4.5	0.7	+6.2	0.6	+5.2	0.6	6
ØR-15	+3.5	0.9	+9.5	0.7	+7.5	1.5	50
ØR-19	+3.7	0.8	+5.9	0.7	+4.7	0.5	29

s.d. standard deviation, *N* number of analyses

albitizing fluid (sample La-8, Fig. 3c, d), and the resulting cracks were filled with minerals of the albitite assemblage. In some cases, the tourmaline was also altered, potentially by the albitizing fluid, as documented by an Fe-rich variety found in an albite-dominated rock at the old mines on the island of Langøy (sample La-14, Fig. 8a, c). Its B isotope signature is similar to the $\delta^{11}B$ values identified for the scapolitizing fluids, which may indicate that tourmaline has been completely replaced during pervasive albitization without significant exchange of B. The mobility of Fe during albitization is further displayed by the co-precipitation of fine-grained hematite, which reddened the feldspar (e.g., sample ØR-14).

The tourmaline crystal in sample La-14 is crisscrossed by Fe-poor but Ca- and Ti-rich tourmaline veins, which represent yet another alteration stage. This latest generation of tourmaline appears in veins related to sericitization of the surrounding albite and contains significantly lighter B isotope signatures of around −1 ‰ (sample La-14, Fig. 8a, c), reflecting a predominantly crustal fluid that again introduced K into the system. Pervasive sericitization of albite was also observed in the tourmaline-bearing albitite samples ØR-14, ØR-15, and ØR-19 from Ringsjø. In sample ØR-15, albite is only slightly sericitized, and the mm-sized tourmaline crystal that was analyzed is highly complex and documents different tourmaline generations. The older part of the crystal is Fe–Al-rich and fractured (Fig. 8b, d). Its B isotope composition ranges from +7 to +9.5 ‰ and is independent of the Fe concentration. However, the secondary growth zone shows a good correlation between Fe content and $\delta^{11}B$ values, which are systematically up to 5 ‰ lighter and match the B isotope signatures of samples ØR-14 and ØR-19. The large tourmaline crystals in samples ØR-14 and ØR-19 are chemically highly variable and show a patchy optical zonation. Their B isotope compositions are however fairly homogeneous at ca. +4 ‰, which suggests a pervasive fluid-induced tourmalinization of a heterogeneous precursor rock. Tourmalinization is also evident in the mineral replacement textures observed in sample E38-3. The orientation of the precursor grains was apparently retained as suggested by variable pleochroism and inherited major-element characteristics (Fig. 5). Such preservation of textural and chemical features of the precursor minerals would demonstrate the close coupling between the dissolution of the parent gabbro and the reprecipitation of the tourmaline and emphasizes the importance of the composition of the interfacial fluid in controlling the tourmaline composition (Putnis 2009). The B isotopes are again fairly homogeneous with a total spread of only 1.4 ‰.

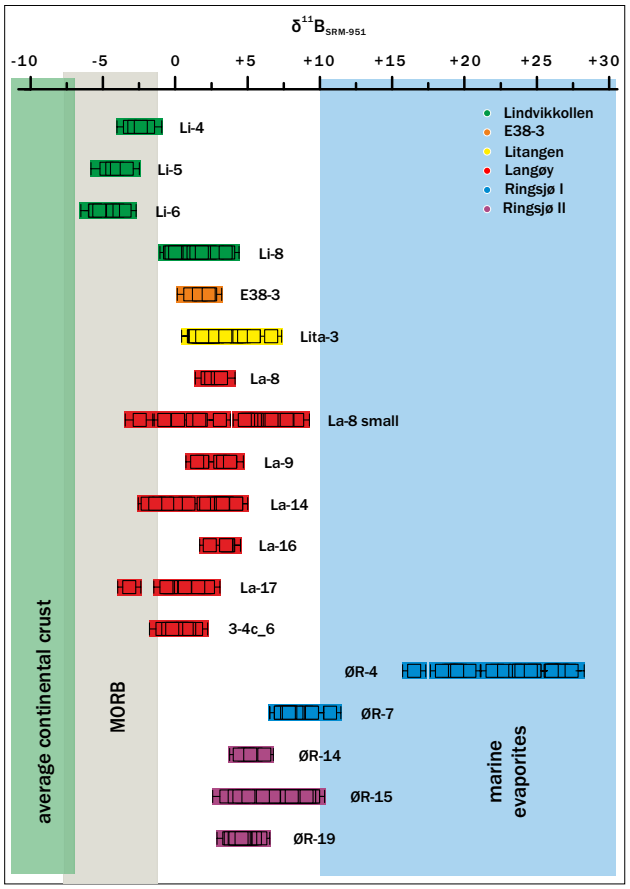

Fig. 6 Regional distribution of the measured tourmaline $\delta^{11}B$ values for all samples compared to typical isotope signatures of different B source reservoirs

Pegmatites

The granite–pegmatite at Lindvikkollen and the amphibolite surrounding it both contain metasomatic tourmaline with slightly negative $\delta^{11}B$ values reflecting the influence of pneumatolytic fluids (samples Li-4, Li-5, and Li-6). However, positive B isotope signatures up to +3.7 ‰ (sample Li-8) clearly indicate mixing with isotopically heavier B from a different source. The major-element chemistry of tourmaline Li-8, which plots along the "oxy-dravite"-povondraite trend, suggests a possible relationship to metaevaporitic fluids. These may have also added K, Mg, and Fe to the system as documented by massive reddened K-feldspar and abundant chlorite veins in sample Li-8. Furthermore, the Sr isotope compositions of tourmaline and albite in sample Li-5 are relatively radiogenic, with initial $^{87}Sr/^{86}Sr$ values around 0.71, which requires a contribution of Sr from an aqueous fluid or melt that was derived from ancient rather than juvenile (i.e., freshly mantle-derived) crust.

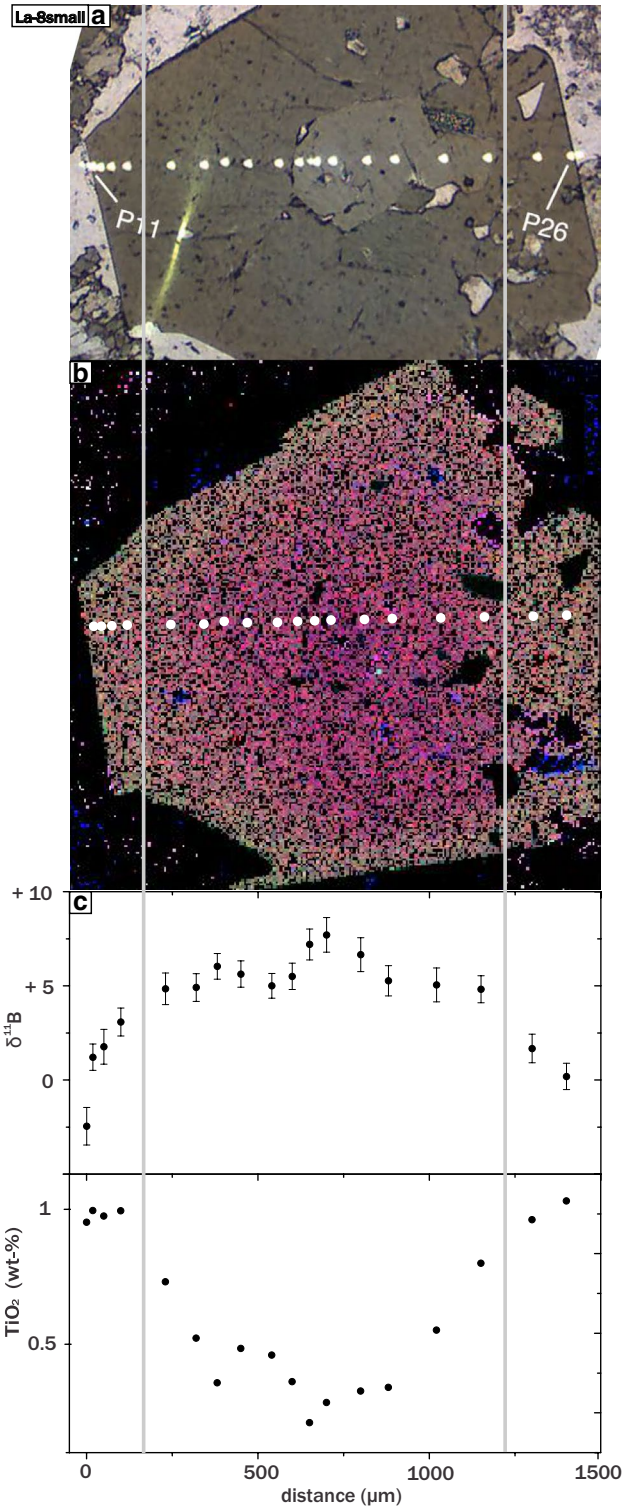

Fig. 7 **a** Thin section image and **b** composite element map (red = Fe, green = Ti, blue = Ca) for tourmaline sample La-8_small (single-element maps for B, Fe, Ca, and Ti can be found in Fig. S2 in the electronic supplementary material), **c** rim-core-rim variation in $\delta^{11}B$ and Ti content

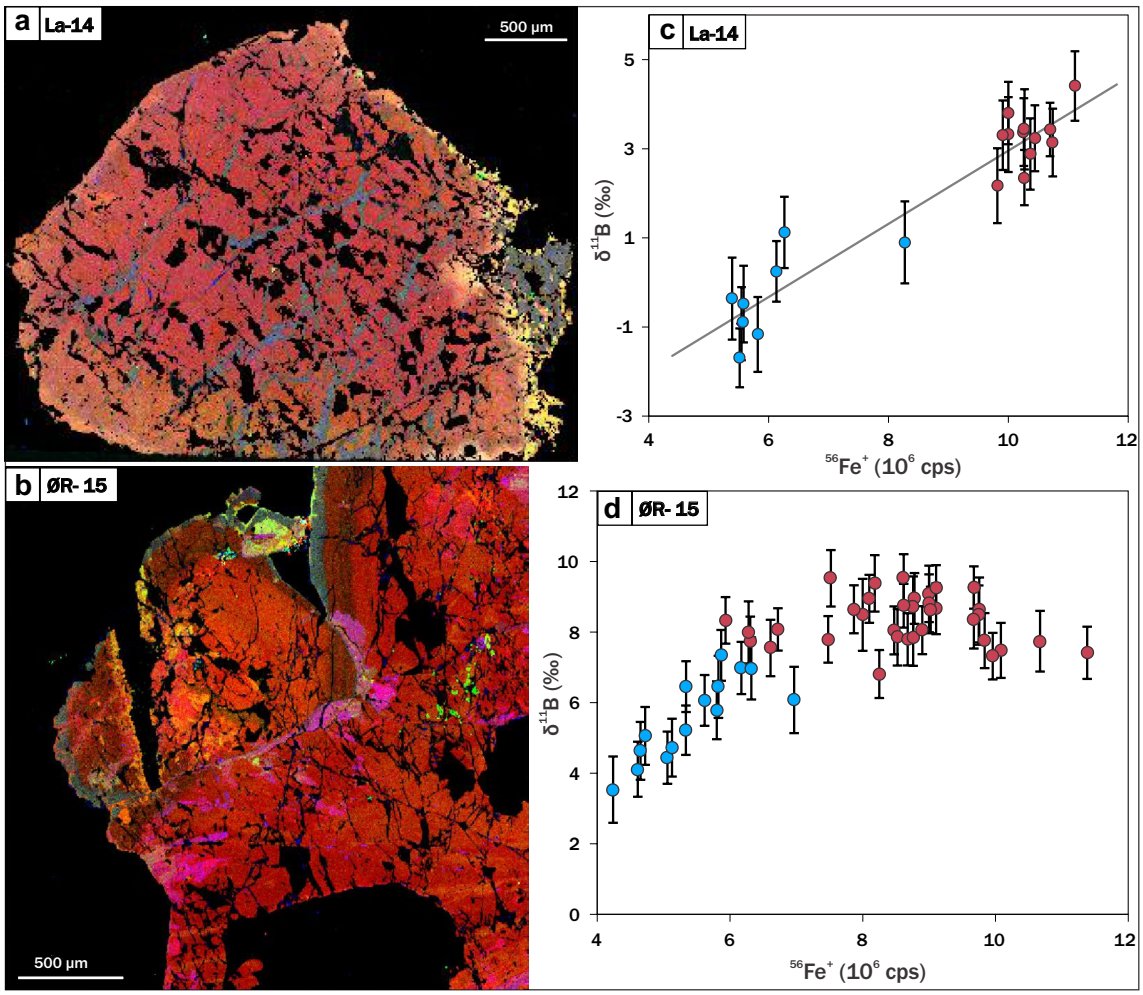

Fig. 8 **a**, **b** Composite element maps (red = Fe, green = Ti, blue = Ca; all non-tourmaline material blacked out) revealing 2 generations of tourmaline with different Fe contents, which **c**, **d** correlate with measured $\delta^{11}B$ values; single-element maps for B, Fe, Ca, and Ti can be found in Fig. S3 (sample La-14) and Fig. S4 (sample ØR-15) in the electronic supplementary material

Regional-scale variations

Different types of metasomatically altered rocks were sampled within 20 km in the Bamble sector, and tourmaline was used as a probe of the hydrothermal fluids. While the tourmaline major-element chemistry may depend on its host rock, its B isotope systematics can be used as a tracer for the fluids. Boron isotope variations on the outcrop scale are typically small and commonly related to different alteration stages as documented by several generations of tourmaline. For the penetrative process of scapolitization, we hypothesize that large amounts of almost homogeneous fluids infiltrated the rocks in the studied field area forming Mg-rich tourmaline with slightly positive $\delta^{11}B$ values. Most tourmaline sampled on the island of Langøy, plus samples Li-8, E38-3, and Lita-3 from other regions belong to this group.

Variations between different outcrops were also observed. Negative $\delta^{11}B$ values in tourmaline from the Lindvikkollen pegmatite reveal the influence of late-stage magmatic fluids. North of the Valle Fault, tourmaline samples from metasedimentary rocks have higher and more variable $\delta^{11}B$ values up to +27.4 ‰ (sample ØR-4). These locally distinct chemical and isotopic compositions seem to depend on local variations in the prevalent sedimentary component which generated the fluid. A systematic sampling campaign in a specific area could help to understand the large-scale relationships between different source rocks in detail.

Implications for possible fluid sources

Metasomatic alteration processes affected large volumes of high-grade metamorphic rocks during a late stage of the Sveconorwegian orogeny as confirmed by the Rb–Sr ages

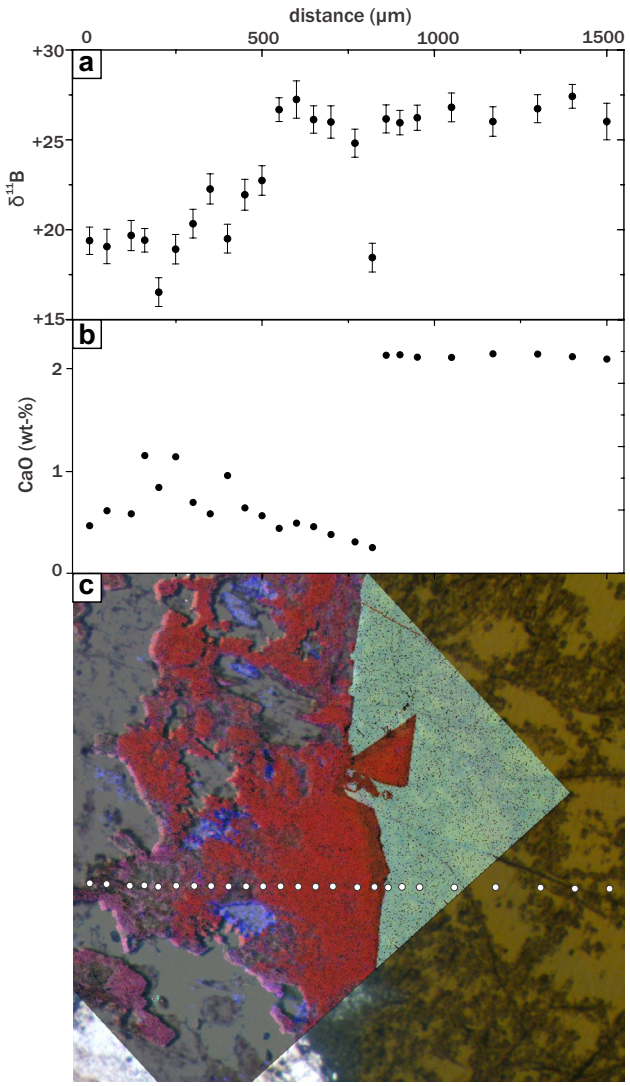

Fig. 9 **a**, **b** Boron isotopes correlate with Ca content in tourmaline sample ØR-4, **c** the 3-element map (red = Fe, green = Ti, blue = Ca) overlay on top of a thin section image indicates the first generation (tur 1, pale *green–blue*, *right* corner of map) with a sharp alteration front, a porous reacted area (tur 2, *red*) and tourmaline overgrowth (tur 3, *purple*); single-element maps for B, Fe, Ca, and Ti of sample ØR-4 can be found in Fig. S5 in the electronic supplementary material

of metasomatic biotite. The estimated upper amphibolite to granulite facies conditions were reached at 1.14–1.12 Ga (Cosca et al. 1998; Bingen et al. 2008a), implying prograde metamorphic dehydration of the Bamble rocks prior to their metasomatic overprint at 1.08–1.04 Ga (Engvik et al. 2011). Therefore, fluids were most likely derived from an external source. The high-grade granite gneisses of Gothian age and gabbros emplaced before the continental collision cannot have generated significant amounts of fluid. Following the model of Bingen et al. (2008b), the high-grade metamorphic Bamble rocks were thrust onto sedimentary units of the adjacent Telemarkia Terrane during uplift and exhumation. These sedimentary units have probably been deposited within a shallow marine environment and may have consisted of a mixture of detrital components, pelagic clays, carbonates, and additionally, evaporites. During the first phase of the Sveconorwegian orogeny, these rocks probably remained at higher crustal levels, e.g., in the upper part of the suggested accretionary wedge, and were then juxtaposed to the exhumed high-grade metamorphic rocks at ~1.08 Ga. Crustal thickening was accompanied by increasing P–T conditions and led to subsequent devolatilization of the Telemarkian sediments, which underwent high-grade metamorphism at 1,035 Ma (Bingen et al. 2008b).

The hydrothermal fluids carried large amounts of Na, Cl, Mg, K, P, and B (Engvik et al. 2008, 2011). The only known source that could provide all these elements at once are evaporites, potentially interlayered with various amounts of pelagic clay and other crustal sources. The sampled orthoamphibole–cordierite rocks were described earlier as potential metaevaporites (Touret 1985). The measured $\delta^{11}B$ values up to +27.4 ‰ in sample ØR-4 now confirm the influence of a marine evaporite-derived component.

Several fluid pulses might be attributed to different stages of dehydration. We hypothesize that sedimentary pore fluids were mobilized first and may have dissolved carbonates and evaporites, resulting in an aggressive fluid that could have triggered the scapolitization and Mg metasomatism of the infiltrated rock units. Subsequent alteration processes typically show ~4 ‰ lighter B isotope signatures and an enrichment in K, and may thus be related to the breakdown of OH-bearing clay minerals at higher P–T conditions.

Conclusions

Tourmaline from the Bamble sector of southern Norway investigated in this study was formed during late-stage orogenic hydrothermal alteration processes. The fluids were highly enriched in elements typically found in seawater such as Na, Cl, Mg, and B as documented by secondary mineral assemblages. Metasomatic tourmaline recorded chemical and isotopic information about the sources of the hydrothermal fluids. The tourmaline $\delta^{11}B$ values indicate variable source reservoirs on a regional scale, as may be found within a sedimentary depositional environment. Heavy B isotope compositions in Mg-rich tourmalines associated with scapolitization imply a seawater-derived component such as marine evaporites. These evaporites may have been intercalated with pelagic clays and continental detritus within a shallow marine environment,

Table 3 Rb-Sr data, the initial $^{87}Sr/^{86}Sr$ is back-calculated to 1,060 Ma

Sample	Mineral	Rb (ppm)	Sr (ppm)	$^{87}Rb/^{86}Sr$	± 2 s.d.	$^{87}Sr/^{86}Sr$ present	2 s.e.	$^{87}Sr/^{86}Sr$ initial
Li-5	tur	2.25	54.3	0.1197	0.0012	0.715143	15	0.713362
	plag	45.3	72.4	1.818	0.018	0.738592	23	0.711551
	bt	496	6.92	299.2	3.0	5.247392	87	0.797248
	hbl	7.75	4.34	5.209	0.052	0.783512	19	0.706021
	wr	110	29.5	10.96	0.11	0.839893	14	(0.676904)
Lita-3	tur	0.0811	71.5	0.003287	0.000033	0.723456	12	0.723407
	mica	228	12.9	55.52	0.56	1.571855	42	0.745933
OR-4	tur	0.176	150	0.003397	0.000034	0.706927	14	0.706877
	K-fsp	101	359	0.8176	0.0082	0.721877	18	0.709715
	ab	184	202	2.652	0.027	0.742486	14	0.703033
	hbl	5.00	14.8	0.9773	0.0098	0.721641	13	0.707103
	bt	276	3.45	353.6	3.5	6.12048	73	0.861142
	wr	104	191	1.582	0.016	0.728820	11	0.705287
La-8	tur	0.274	303	0.002614	0.000026	0.703550	13	0.703511
	ep	1.39	3,480	0.001153	0.000011	0.706198	23	0.706181
	amph	6.58	45.8	0.4156	0.0042	0.710128	18	0.703946
	bt	254	9.52	87.22	0.87	2.015690	4	0.718262
	wr	43.8	480	0.2645	0.0026	0.709999	11	0.706064
ØR-19	tur	6.91	176	0.1135	0.0011	0.707905	16	0.706217
	ab	153	192	2.307	0.023	0.742422	21	0.708105
ØR-20	scp	9.74	248	0.1134	0.0011	0.707577	18	0.705890
	bt	426	3.90	582.4	5.8	9.304660	19	(0.641254)
	wr	72.6	18.1	11.79	0.12	0.869607	31	(0.694227)

tur tourmaline, *plag* plagioclase, *bt* biotite, *hbl* hornblende, *wr* whole rock, *mica* white mica, *K-fsp* K-feldspar, *ab* albite, *ep* epidote, *amph* amphibole, *scp* scapolite; samples ØR-19 and ØR-20 are from a single rock. For $^{87}Sr/^{86}Sr$, stated analysis uncertainties refer to the least significant digits

resulting in locally variable $\delta^{11}B$ signatures within the source reservoir. Subsequent fluid pulses (e.g., albitizing, then sericitizing fluids) and their chemical variety may be ascribed to different stages of dehydration, as sedimentary pore fluids will be released early on at low P–T conditions, and evaporites may be mobilized before the breakdown of OH-bearing clay minerals occurs.

Metasomatism converted existing minerals into tourmaline, or existing tourmaline reacted in the presence of a fluid of suitable composition to a tourmaline of different chemical composition. During the replacement process, the B budget was dominated by the precursor tourmaline, whereas some of the other major elements were strongly influenced by the infiltrating fluid. New tourmaline overgrowths require the addition of B, and these overgrowths have an isotope composition dominated by the fluid. Detailed petrographic investigations revealed different stages in the alteration history recorded by several tourmaline generations. The Sr isotope compositions of tourmaline and coexisting minerals enabled us to assign tourmaline formation to distinct metasomatic events, demonstrating the potential of combined isotope investigations.

The different episodes of mineral formation and replacement were enabled by fluids of different compositions that were generated during the Sveconorwegian orogeny. These fluids were derived episodically from different rock units associated with the Bamble sector. A key role can be attributed to a source containing marine evaporites and pelitic continental detritus. These observations demonstrate the importance of large quantities of fluids, their specific compositions, and their large-scale mobility on the resulting mineral assemblages and the major chemical changes that can occur during regional metamorphism.

Acknowledgments This study was funded by the Gottfried Wilhelm Leibniz Award of the Deutsche Forschungsgemeinschaft to KM. The paper emerged from the Master's thesis of the first author written at the Institut für Mineralogie, Westfälische Wilhelms-Universität Münster. Technical support in the clean laboratory facilities and during TIMS analyses was given by Heidi Baier. Ane Engvik provided useful information about tourmaline sample localities. RB thanks Christof Kusebauch for fruitful discussions and Jasper Berndt-Gerdes for assistance with the electron microprobe. We thank C.-J. De Hoog and an anonymous reviewer for their constructive comments, and J. Touret for editorial handling of the manuscript.

References

Agostini S, Ryan JG, Tonarini S, Innocenti F (2008) Drying and dying of a subducted slab: coupled Li and B isotope variations in Western Anatolia Cenozoic Volcanism. Earth Planet Sci Lett 272:139–147

Åhäll KI, Cornell DH, Armstrong R (1998) Ion probe zircon dating of metasedimentary units across the Skagerrak: new constraints for

early Mesoproterozoic growth of the Baltic Shield. Precambrian Res 87:117–134

Alirezaei S, Cameron EM (2002) Mass balance during gabbro-amphibolite transition, Bamble Sector, Norway: implications for petrogenesis and tectonic setting of the gabbros. Lithos 60:21–45

Armstrong JT (1988) Quantitative analysis of silicate and oxide materials: comparison of Monte Carlo, ZAF, and φ(ρZ) procedures. In: Newbury DE (ed) Microbeam analysis. San Francisco Press, Inc., San Francisco, CA, USA, pp 239–246

Armstrong JT (1991) Quantitative elemental analysis of individual microparticles with electron beam instruments. In: Heinrich KFJ, Newbury DE (eds) Electron probe quantitation. Plenum Press, New York, pp 261–315

Austrheim H, Putnis CV, Engvik AK, Putnis A (2008) Zircon coronas around Fe–Ti oxides: a physical reference frame for metamorphic and metasomatic reactions. Contrib Mineral Petrol 156:517–527

Baadsgaard H, Chaplin C, Griffin WL (1984) Geochronology of the Gloserheia pegmatite, Froland, southern-Norway. Norsk Geol Tidsskr 64:111–119

Barth S (1993) Boron isotope variations in nature—a synthesis. Geol Rundsch 82:640–651

Bebout GE, Nakamura E (2003) Record in metamorphic tourmalines of subduction-zone devolatilization and boron cycling. Geology 31:407–410

Bingen B, Davis WJ, Hamilton MA, Engvik AK, Stein HJ, Skar O, Nordgulen O (2008a) Geochronology of high-grade metamorphism in the Sveconorwegian belt, S. Norway: U–Pb, Th–Pb and Re–Os data. Nor J Geol 88:13–42

Bingen B, Nordgulen O, Viola G (2008b) A four-phase model for the Sveconorwegian orogeny, SW Scandinavia. Nor J Geol 88:43–72

Brøgger, WC (1906) Die Mineralen der südnorwegischen Granit-Pegmatitgänge. I Det Norske Videnskaps-Akademi I Oslo Skrifter, Matematisk-Naturvidenskapelig Klasse 1906-6

Catanzaro FJ, Champion CE, Garner EL, Marinenko G, Sappenfield KM, Shields WR (1970) Boric acid; isotopic and assay standard reference materials. NBS (US) Special Publication 260-17, 70

Chaussidon M, Albarède F (1992) Secular boron isotope variations in the continental-crust—an ion microprobe study. Earth Planet Sci Lett 108:229–241

Clift PD, Layne G, Najman YMR, Kopf A, Shimizu N, Hunt J (2003) Termporal evolution of boron flux in the NE Japan and Izu arcs measured by ion microprobe from the forearc tephre record. J Petrol 44:1211–1236

Cosca MA, Mezger K, Essene EJ (1998) The Baltica–Laurentia connection: Sveconorwegian (Grenvillian) metamorphism, cooling, and unroofing in the Bamble sector, Norway. J Geol 106:539–552

de Haas GJLM, Verschure RH, Maijer C (1993) Isotopic constraints on the timing of crustal accretion of the Bamble sector, Norway, as evidenced by coronitic gabbros. Precam Res 64:403–417

de Haas GJLM, Andersen T, Vestin J (1999) Detrital zircon geochronology: new evidence for an old model for accretion of the southwest Baltic Shield. J Geol 107:569–586

Dutrow BL, Foster CT, Henry DJ (1999) Tourmaline-rich pseudomorphs in sillimanite zone metapelites: demarcation of an infiltration front. Am Mineral 84:794–805

Dyar MD, Wiedenbeck M, Robertson D, Cross LR, Delaney JS, Ferguson K, Francis CA, Grew ES, Guidotti CV, Hervig RL, Hughes JM, Husler J, Leeman W, McGuire AV, Rhede D, Rothe H, Paul RL, Richards I, Yates M (2001) Reference minerals for the microanalysis of light elements. Geostand Newsl 25:441–463

Engvik AK, Austrheim H (2010) Formation of sapphirine and corundum in scapolitised and Mg-metasomatised gabbro. Terra Nova 22:166–171

Engvik AK, Putnis A, Fitz Gerald JD, Austrheim H (2008) Albitization of granitic rocks; the mechanism of replacement of oligoclase by albite. Can Mineral 46:1401–1415

Engvik AK, Golla-Schindler U, Berndt J, Austrheim H, Putnis A (2009) Intragranular replacement of chlorapatite by hydroxy-fluor-apatite during metasomatism. Lithos 112:236–246

Engvik AK, Mezger K, Wortelkamp S, Bast R, Corfu F, Korneliussen A, Ihlen P, Austrheim H, Bingen B (2011) Metasomatism of gabbro—mineral replacement and element mobilization during the Sveconorwegian metamorphic event. J Metamorph Geol 29:399–423

Foster GL, Pogge von Strandmann PAE, Rae JWB (2010) Boron and magnesium isotopic composition of seawater. Geochem Geophys Geosyst 11:Q08015

Harlov DE (2000) Pressure-temperature estimation in orthopyroxene-garnet bearing granulite facies rocks, Bamble sector, Norway. Mineral Petrol 69:11–33

Harlov DE, Forster HJ, Nijland TG (2002) Fluid-induced nucleation of (Y + REE)-phosphate minerals within apatite: nature and experiment. Part I. Chlorapatite. Am Mineral. Am Mineral 87:245–261

Hemming NG, Hanson GN (1992) Boron isotopic composition and concentration in modern marine carbonates. Geochim Cosmochim Acta 56:537–543

Henry DJ, Dutrow BL (1996) Metamorphic tourmaline and its petrologic applications. Rev Mineral Geochem 33:503–557

Henry DJ, Guidotti CV (1985) Tourmaline as a petrogenetic indicator mineral—an example from the staurolite-grade metapelites of NW maine. Am Mineral 70:1–15

Henry DJ, Sun H, Slack JF, Dutrow BL (2008) Tourmaline in metaevaporites and highly magnesian rocks: perspectives from Namibian tourmalinites. Eur J Mineral 20:889–904

Henry DJ, Novak M, Hawthorne FC, Ertl A, Dutrow BL, Uher P, Pezzotta F (2011) Nomenclature of the tourmaline-supergroup minerals. Am Mineral 96:895–913

Hövelmann J, Austrheim H, Putnis A (2014) Cordierite formation during the experimental reaction of plagioclase with Mg-rich aqueous solutions. Contrib Mineral Petrol 168. doi:10.1007/s00410-014-1063-x

Ishikawa T, Nakamura E (1993) Boron isotope systematics of marine-sediments. Earth Planet Sci Lett 117:567–580

Kakihana H, Kotaka M, Satoh S, Nomura M, Okamoto M (1977) Fundamental studies on ion-exchange separation of boron isotopes. Bull Chem Soc Jpn 50:158–163

Kasemann SA, Prave AR, Fallick AE, Hawkesworth CJ, Hoffmann K (2010) Neoproterozoic ice ages, boron isotopes, and ocean acidification: implications for a snowball Earth. Geology 38:775–778

King RW, Kerrich RW (1989) Strontium isotope compositions of tourmaline from lode gold deposits of the Archean Abitibi Greenstone-Belt (Ontario Quebec, Canada)—implications for source reservoirs. Chem Geol 79:225–240

Klemme S, Marschall HR, Jacob DE, Prowatke S, Ludwig T (2011) Trace-element partitioning and boron isotope fractionation between white mica and tourmaline. Can Mineral 49:165–176

Knudsen TL, Andersen T (1999) Petrology and geochemistry of the Tromoy gneiss complex, South Norway, an alleged example of Proterozoic depleted lower continental crust. J Petrol 40:909–933

Knudsen TL, Andersen T, Whitehouse MJ, Vestin J (1997) Detrital zircon ages from southern Norway—implications for the Proterozoic evolution of the southwestern Baltic shield. Contrib Mineral Petrol 130:47–58

Korneliussen A, Furuhaug L (2000) On the rutile deposits Ramsgrønova, Orkhiea, Ødegården and Lindvikkollen, S. Norway. NGU Report 2000.123

Kusebauch C, John T, Barnes J, Klügel A, Austrheim H (2014) Applying halogen data and δ^{37}Cl values to decipher the fluid evolution during regional metasomatism (Bamble sector SE Norway). Submitted to J Petrol

Larsen KE (2008) Lindvikskollen-Kalstadgangen, Kragerø, en klassisk Norsk granittpegmatitt. Nor Bergv Mus Skr 38:37–44

Leeman WP, Tonarini S (2001) Boron isotopic analysis of proposed borosilicate mineral reference samples. Geostand Newsl 25:399–403

Lieftink DJ, Nijland TG, Maijer C (1994) The behavior of rare-earth elements in high-temperature cl-bearing aqueous fluids—results from the Odegardens-Verk natural laboratory. Can Mineral 32:149–158

London D, Kontak DJ (2012) Granitic pegmatites: scientific wonders and economic bonanzas. Elements 8:257–261

Ludwig KR (2009) Isoplot, Berkeley Geochronology Center, version 3.72.09.12.09

Ludwig T, Marschall HR, Pogge von Strandmann PAE, Shabaga BM, Fayek M, Hawthorne FC (2011) A secondary ion mass spectrometry (SIMS) re-evaluation of B and Li isotopic compositions of Cu-bearing elbaite from three global localities. Mineral Mag 75:2485–2494

MacGregor JR, Grew ES, De Hoog JCM, Harley SL, Kowalski PM, Yates MG, Carson CJ (2013) Boron isotopic composition of tourmaline, prismatine, and grandidierite from granulite facies paragneisses in the Larsemann Hills, Prydz Bay, East Antarctica: evidence for a non-marine evaporate source. Geochim Cosmochim Acta 123:261–283

Marks MAW, Marschall HR, Schühle P, Guth A, Wenzel T, Jacob DE, Barth M, Markl G (2013) Trace element systematics of tourmaline in pegmatitic and hydrothermal systems from the Variscan Schwarzwald (Germany): the importance of major element composition, sector zoning, and fluid or melt composition. Chem Geol 344:73–90

Marschall HR, Jiang SY (2011) Tourmaline isotopes: no element left behind. Elements 7:313–319

Marschall HR, Ludwig T, Altherr R, Kalt A, Tonarini S (2006) Syros metasomatic tourmaline: evidence for very high-delta B-11 fluids in subduction zones. J Petrol 47:1915–1942

Marschall HR, Altherr R, Kalt A, Ludwig T (2008) Detrital, metamorphic and metasomatic tourmaline in high-pressure metasediments from Syros (Greece): intra-grain boron isotope patterns determined by secondary-ion mass spectrometry. Contrib Mineral Petrol 155:703–717

Marschall HR, Meyer C, Wunder B, Ludwig T, Heinrich W (2009a) Experimental boron isotope fractionation between tourmaline and fluid: confirmation from in situ analyses by secondary ion mass spectrometry and from Rayleigh fractionation modelling. Contrib Mineral Petrol 158:675–681

Marschall HR, Korsakov AV, Luvizotto GL, Nasdala L, Ludwig T (2009b) On the occurrence and boron isotopic composition of tourmaline in (ultra)high-pressure metamorphic rocks. J Geol Soc 166:811–823

Mercadier J, Richard A, Cathelineau M (2012) Boron- and magnesium-rich marine brines at the origin of giant unconformity-related uranium deposits: $\delta^{11}B$ evidence from Mg-tourmalines. Geology 40:231–234

Meyer C, Wunder B, Meixner A, Romer RL, Heinrich W (2008) Boron-isotope fractionation between tourmaline and fluid: an experimental re-investigation. Contrib Mineral Petrol 156:259–267

Moine B, Sauvan P, Jarousse J (1981) Geochemistry of evaporite-bearing series—a tentative guide for the identification of metaevaporites. Contrib Mineral Petrol 76:401–412

Morgan GB, London D (1989) Experimental reactions of amphibolite with boron-bearing aqueous fluids at 200 Mpa: implications for tourmaline stability and partial melting in mafic rocks. Contrib Mineral Petrol 102:281–297

Mueller AG, Delaeter JR, Groves DI (1991) Strontium isotope systematics of hydrothermal minerals from epigenetic archean gold deposits in the Yilgarn Block, Western Australia. Econ Geol Bull Soc Econ Geol 86:780–809

Munz IA (1990) Whiteschists and orthoamphibole cordierite rocks and the P–T–t path of the Modum Complex, South Norway. Lithos 24:181–199

Munz IA, Morvik R (1991) Metagabbros in the Modum Complex, Southern Norway—an important heat-source for Sveconorwegian metamorphism. Precambrian Res 52:97–113

Munz IA, Wayne D, Austrheim H (1994) Retrograde fluid infiltration in the high-grade Modum Complex, South Norway—evidence for age, source and REE mobility. Contrib Mineral Petrol 116:32–46

Nakano T, Nakamura E (2001) Boron isotope geochemistry of metasedimentary rocks and tourmalines in a subduction zone metamorphic suite. Phys Earth Planet Inter 127:233–252

Nebel O, Mezger K, Scherer EE (2011) Evaluation of the ^{87}Rb decay constant by age comparison against the U–Pb system. Earth Planet Sci Lett 301:1–8

Nijland TG, Maijer C, Senior A, Verschure RH (1993) Primary sedimentary structures and composition of the high-grade metamorphic Nivelda Quartzite Complex [Bamble, Norway], and the origin of nodular gneisses. Proc Koninklijke Nederlandse Akademie Van Wetenschappen-Biol Chem Geol Phys Med Sci 96:217–232

Nijland TG, Harlov DE, Andersen T (2014) The Bamble sector, South Norway: a review. Geosci Front 5:635–658

O'Nions RK, Baadsgaard H (1971) Radiometric study of polymetamorphism in Bamble Region, Norway. Contrib Mineral Petrol 34:1–21

Padget P (2004) Metasedimentary rocks, associated intrusions and tectonic features of the Precambrian in eastern Bamble, South Norway: an interpretative study. NGU Bull 441:39–51

Padget P, Brekke H (1996) Geologisk kart over Norge, berggrunnskart Arendal - 1:250 000. Geological Survey of Norway, Trondheim

Palmer MR (1991) Boron isotope systematics of hydrothermal fluids and tourmalines—a synthesis. Chem Geol 94:111–121

Palmer MR, Slack JF (1989) Boron isotopic composition of tourmaline from massive sulfide deposits and tourmalinites. Contrib Mineral Petrol 103:434–451

Palmer MR, Swihart GH (1996) Boron isotope geochemistry: an overview. Rev Mineral Geochem 33:709–744

Palmer MR, Spivack AJ, Edmond JM (1987) Temperature and pH controls over isotopic fractionation during adsorption of boron on marine clay. Geochim Cosmochim Acta 51:2319–2323

Papanastassiou DA, Wasserburg GJ (1969) Initial strontium isotopic abundances and the resolution of small time differences in the formation of planetary objects. Earth Planet Sci Lett 5:361–376

Pesquera A, Torres-Ruiz J, Garcia-Casco A, Gil-Crespo PP (2013) evalutating the controls on tourmaline formation in granitic systems: a case study on peraluminous granites from the Central Iberian Zone (CIZ), Western Spain. J Petrol 54:609–634

Putnis A (2009) Mineral replacement reactions. Rev Mineral Geochem 70:87–124

Putnis A, Hinrichs R, Putnis CV, Golla-Schindler U, Collins LG (2007) Hematite in porous red-clouded feldspars: evidence of large-scale crustal fluid-rock interaction. Lithos 95:10–18

Schwarcz HP, Agyei EK, Mccmulle CC (1969) Boron isotopic fractionation during clay adsorption from sea-water. Earth Planet Sci Lett 6:1–5

Shields G, Veizer J (2002) Precambrian marine carbonate isotope database: version 1.1. Geochem Geophys Geosyst 3:1031

Smalley PC, Field D, Lamb RC, Clough PWL (1983) Rare-earth, Th-Hf-Ta and large-ion lithophile element variations in metabasites from the Proterozoic amphibolite-granulite transition zone at Arendal, South-Norway. Earth Planet Sci Lett 63:446–458

Spivack AJ, Palmer MR, Edmond JM (1987) The sedimentary cycle of the boron isotopes. Geochim Cosmochim Acta 51:1939–1949

Swihart GH, Moore B, Callis EL (1986) Boron isotopic composition of marine and nonmarine evaporite borates. Geochim Cosmochim Acta 50:1297–1301

Tonarini S, Forte C, Petrini R, Ferrara G (2003) Melt/biotite 11B/10B isotope fractionation and the boron local environment in the structure of volcanic glasses. Geochim Cosmochim Acta 67:1863–1873

Touret JLR (1985) Fluid regime in southern Norway: the record of fluid inclusions. In: Tobi AC, Touret JLR (eds) The deep proterozoic crust in the North Atlantic Provinces. Reidel, Dordrecht, pp 517–549

Van Hinsberg VJ, Henry DJ, Marschall H (2011) Tourmaline: an ideal indicator of its host environmrent. Can Mineral 49:1–16

Vengosh A, Starinsky A, Kolodny Y, Chivas AR, Raab M (1992) Boron isotope variations during fractional evaporation of seawater—new constraints on the marine vs nonmarine debate. Geology 20:799–802

Visser D (1995) Kornerupine in a biotite-spinel-garnet schist near Böylefossbru, Bamble sector, south Norway: implications for early and late metamorphic fluid activity. Neues Jahrb Miner Abh 169:1–34

Visser D, Kloprogge JT, Maijer C (1994) An Infrared spectroscopic (Ir) and light-element (Li, Be, Na) study of cordierites from the Bamble Sector, South Norway. Lithos 32:95–107

Visser D, Nijland TG, Lieftink DJ, Maijer C (1999) The occurrence of preiswerkite in a tourmaline-biotite-scapolite rock from Blengsvatn, Norway. Am Mineral 84:977–982

Xavier RP, Wiedenbeck M, Trumbull RB, Dreher AM, Monteiro LVS, Rhede D, de Araujo CEG, Torresi I (2008) Tourmaline B-isotopes fingerprint marine evaporites as the source of high-salinity ore fluids in iron oxide copper-gold deposits, Carajas Mineral Province (Brazil). Geology 36:743–746